This material has been copied
under licence from CANCOPY.
Resale or further copying of this material is
strictly prohibited.

Le présent document a été reproduit
avec l'autorisation de CANCOPY.
La revente ou la reproduction ultérieure
en sont strictement interdites.

DP-1122

LIBRARY
Copy 4
APR 30 1968
ATOMIC ENERGY OF CANADA LIMITED

AEC RESEARCH AND DEVELOPMENT REPORT

LATTICE EXPERIMENTS WITH SIMULATED BURNED-UP FUEL FOR D_2O POWER REACTORS

N. P. BAUMANN
J. L. CRANDALL
R. L. OLSON
G. F. O'NEILL
D. J. PELLARIN
V. D. VANDERVELDE

DUPONT
REG. U. S. PAT. OFF.

Savannah River Laboratory

Aiken, South Carolina

LEGAL NOTICE

This report was prepared as an account of Government sponsored work. Neither the United States, nor the Commission, nor any person acting on behalf of the Commission:

A. Makes any warranty or representation, expressed or implied, with respect to the accuracy, completeness, or usefulness of the information contained in this report, or that the use of any information, apparatus, method, or process disclosed in this report may not infringe privately owned rights; or

B. Assumes any liabilities with respect to the use of, or for damages resulting from the use of any information, apparatus, method, or process disclosed in this report.

As used in the above, "person acting on behalf of the Commission" includes any employee or contractor of the Commission, or employee of such contractor, to the extent that such employee or contractor of the Commission, or employee of such contractor prepares, disseminates, or provides access to, any information pursuant to his employment or contract with the Commission, or his employment with such contractor.

Printed in the United States of America
Available from
Clearinghouse for Federal Scientific and Technical Information
National Bureau of Standards, U. S. Department of Commerce
Springfield, Virginia 22151
Price: Printed Copy $3.00; Microfiche $0.65

DP-1122

Reactor Technology
(TID-4500)

LATTICE EXPERIMENTS WITH SIMULATED BURNED-UP FUEL FOR D_2O POWER REACTORS

by

N. P. Baumann
J. L. Crandall
R. L. Olson
G. F. O'Neill
D. J. Pellarin
V. D. Vandervelde

Approved by

J. L. Crandall, Research Manager
Experimental Physics Division

February 1968

E. I. DU PONT DE NEMOURS & COMPANY
SAVANNAH RIVER LABORATORY
AIKEN, S. C. 29801

CONTRACT AT(07-2)-1 WITH THE
UNITED STATES ATOMIC ENERGY COMMISSION

ABSTRACT

The changes in lattice physics parameters accompanying fuel burnup in natural-uranium-fueled D_2O power reactors were studied by measuring bucklings and neutron reaction rates for D_2O-moderated lattices of UO_2 rod clusters containing five different concentrations of ^{235}U and the plutonium isotopes. Both 19- and 31-rod clusters with D_2O, gas, and organic coolants were used at triangular lattice pitches of 9.33 and 12.12 inches. Substitution measurements in natural UO_2 lattices in the Process Development Pile determined the uniform lattice bucklings. Exponential measurements in the Subcritical Experiment determined the changes in buckling induced by uniform lattice heating.

Foil activations, also performed in the Subcritical Experiment, measured the thermal neutron distributions in terms of Mn activations, the thermal neutron spectral indices in terms of Lu-Mn and ^{239}Pu-^{235}U activations, resonance neutron capture in ^{238}U in terms of the cadmium ratio for ^{239}Np production, fast fissions in ^{238}U and all fissions in ^{235}U in terms of the induced fission product activities, and fissile material conversion ratios in terms of the ^{238}U capture to ^{235}U fission ratios.

These results were compared with calculations by the HAMMER code, a one-dimensional, integral-transport cell calculation performed in 84 energy groups. Although agreement between experiment and theory was in general good, significant discrepancies were observed in the spectral index and resonance capture calculations. These discrepancies were tentatively assigned primarily to difficulties in reducing the highly heterogeneous fuel clusters into a ring model for the one-dimensional calculations.

CONTENTS

	Page
List of Tables	4
List of Figures	5
Introduction	7
Summary	9
Discussion	11
Description of the Fuel Assemblies	11
Special Irradiation Rods	14
Fuel Types A, B, C, and D Irradiation Rods	14
Natural Uranium Oxide Irradiation Rods (Type E)	14
Buckling Measurements	16
The PDP Facility	16
Lattice Bucklings by Substitution	16
Temperature Coefficient Measurements	22
The SE-SP Facility	22
Buckling Measurements in the SE	22
Activation Experiments	24
Foil Loadings	24
Resonance Capture	28
Fast Fission Effect	30
Neutron Spectral Index	31
Intracell Flux Profiles	32
Computation of Lattice Parameters	45
Lattice Computations - Cylindrical Model	45
Comparison of Experiment to Theory	50
PDP Bucklings	50
SE Temperature Coefficients	50
Activation Experiments	50
Thermal Neutron Temperature Index	55
Fast Fission Effect	60
Resonance Capture	62
Appendix A	63
Chemical and Isotopic Analyses	63
Appendix B	65
Uniformity of Plutonium Distribution	65
Appendix C	67
Substitution Buckling Measurements	67
Bibliography	73

LIST OF TABLES

Table		Page
I	Assay of Fuel Pellets	12
II	Impurity Analyses of PuO_2-UO_2 Fuels	13
III	PDP Reference Lattice Data	17
IV	Material Bucklings from Analysis of PDP Substitutions	21
V	Description of Foils and Gamma Counting Procedures	25
VI	Resonance Capture and Fast Fission in Clusters of Uranium Oxide Rods	29
VII	Foil Activations for 19-Rod Clusters of Type A Fuel with D_2O Coolant (99.57 mol % D_2O Coolant and Moderator)	33
VIII	Foil Activations for 19-Rod Clusters of Type B Fuel with HB-40 Coolant (99.48 mol % D_2O Moderator)	34
IX	Foil Activations for 19-Rod Clusters of Type C Fuel with HB-40 Coolant (99.65 mol % D_2O Moderator)	35
X	Foil Activations for 19-Rod Clusters of Type C Fuel with D_2O Coolant (99.66 mol % D_2O Coolant and Moderator)	36
XI	Foil Activations for 19-Rod Clusters of Type C Fuel with Air Coolant (99.66 mol % D_2O Moderator)	37
XII	Foil Activations for 19-Rod Clusters of Type E Fuel with HB-40 Coolant (99.64 mol % D_2O Moderator)	38
XIII	Foil Activations for 19-Rod Clusters of Type E Fuel with D_2O Coolant (99.65 mol % D_2O Coolant and Moderator)	39
XIV	Foil Activations for 19-Rod Clusters of Type E Fuel with Air Coolant (99.66 mol % D_2O Moderator)	40
XV	Foil Activations for 31-Rod Clusters of Type C Fuel with D_2O Coolant (99.63 mol % D_2O Coolant and Moderator)	41
XVI	Foil Activations for 31-Rod Clusters of Type C Fuel with HB-40 Coolant (99.61 mol % D_2O Moderator)	42
XVII	Foil Activations for 31-Rod Clusters of Type E Fuel with D_2O Coolant (99.63 mol % D_2O Coolant and Moderator)	43
XVIII	Foil Activations for 31-Rod Clusters of Type E Fuel with HB-40 Coolant (99.59 mol % D_2O Moderator)	44
XIX	Computed ρ Values for Different Fuel Cluster Models	46
XX	SRL Ring Models of 19- and 31-Rod Clusters	48
XXI	HAMMER Calculations of Test Lattices	49
XXII	Comparison of Different Chemical Assays of Type A Fuel	63

LIST OF TABLES (Continued)

Table		Page
XXIII	Summary of Plutonium Analyses for Fuel Types A, B, and C	64
XXIV	Summary of PDP Measured Bucklings by Different Methods of Analysis	68
XXV	Critical Water Heights, Temperature, and Moderator Purity Corrections for PDP Substitution Measurements	69

LIST OF FIGURES

Figure		
1	Fuel Rod Types	12
2	Fuel Cluster Arrangement	13
3	Thin-Walled UO_2-PuO_2 Irradiation Capsule	15
4	Typical Loading of PDP for Substitution Buckling Measurements	19
5	Temperature Coefficient of the Lattice Buckling	23
6	Schematic of Foil Loading in UO_2-PuO_2 Lattice Measurements	25
7	Schematic of Typical Foil Loading in Natural Uranium (Type E) Lattices	26
8	SE Face Map for Irradiation Experiments	26
9	Reference Flux Positions for Activation Experiments	27
10	SRL Concentric Ring Model for HAMMER Computations	47
11	HAMMER Computation of Intracell Flux Profile Showing Sensitivity to Ring Model Used	47
12	Comparison of Computed to Measured Bucklings	51
13	Thermal Neutron Activation Profiles for 19-Rod Clusters	52
14	Thermal Neutron Activation Profiles for 31-Rod Clusters	53
15	Lu-Mn Neutron Temperature Index Profiles for 19-Rod Clusters	56
16	Lu-Mn Neutron Temperature Index Profiles for 31-Rod Clusters	57
17	^{239}Pu-^{235}U Neutron Temperature Index Profiles for 19-Rod Clusters	58
18	^{239}Pu-^{235}U Neutron Temperature Index Profiles for 31-Rod Clusters	59
19	Comparison of HAMMER Spectrum to Westcott Model	61
20	Assay of Plutonium Agglomeration in Type A Fuel	66

INTRODUCTION

The experiments described in this report are part of the USAEC-AECL Cooperative Program of research and development on D_2O-moderated power reactors. They were undertaken to determine the basic changes in lattice physics parameters that accompany plutonium buildup at high fuel burnups in natural-uranium-fueled D_2O power reactors.

Mockups of partially burned natural UO_2 fuel rods were prepared by coprecipitating mixtures of plutonium and uranium depleted in ^{235}U. The mixed oxides were formed into pellets, fired, ground to 0.500-inch diameter, and loaded into aluminum tubes. Five fuel types were made as listed below:

Fuel Type	Isotopic Composition, wt% of total U + Pu					
	^{235}U	^{238}U	^{239}Pu	^{240}Pu	^{241}Pu	^{242}Pu
A	0.30	99.388	0.24	0.062	0.009	0.001
B	0.30	99.431	0.25	0.016	0.002	0.001
C	0.30	99.324	0.35	0.023	0.002	0.001
D	0.50	99.500	0.00	0.00	0.00	0.00
E	0.712	99.288	0.00	0.00	0.00	0.00

Three of the fuels, Types A, B, and C, contain different isotopic mixtures of plutonium over the range of values expected for fuel burnups up to 5000 MWD/ton, while the last two fuels, Types D and E, respectively, consist of depleted uranium and natural uranium alone. Fuel Types A through D were fabricated by Nuclear Fuel Services, Erwin, Tennessee. The natural uranium fuel, available in considerably larger quantities, had been fabricated previously by the General Electric Company, San Jose, California.[1]

The fuel rods were assembled into 19- and 31-rod clusters for the experiments. The plutonium was uniformly mixed with the uranium in the Types A, B, and C fuel, i.e., no attempt was made to mock up the very complex isotopic distribution resulting from fuel burnup in an actual rod cluster. The uniform mixture provided the advantage of a relatively simple system for comparison with calculations.

The experiments with these fuel assemblies were performed in the Process Development Pile (PDP)[2], a zero-power D_2O lattice test facility 16 feet 2-3/4 inches in diameter with an effective height of 15 ft, and in the Subcritical Experiment (SE)[3], a D_2O exponential 5 ft in diameter and 7 ft high. The neutron feed for the SE was supplied by the Standard Pile (SP), a small graphite test reactor. Thermal neutron fluxes up to 10^8 n/(cm^2)(sec) were available in the SE for the foil activation measurements.

SUMMARY

Substitution buckling measurements on the simulated burned-up fuel assemblies were performed in the PDP. Natural UO_2 rod clusters of the same dimensions and at the same lattice pitch as the test clusters were used for the host lattice. Measurements were made on 19- and 31-rod clusters at 9.33- and 12.12-inch triangular lattice pitches with D_2O, HB-40, and gas as the cluster coolant. Lattice bucklings varied from -4.75 to +7.25 m^{-2}. The substitution measurements were analyzed by two-group, two-region diffusion theory calculation[4], by a successive substitution method[5], and by a heterogeneous reactor code[6]. All the analysis methods gave consistent results, with the heterogeneous analysis adjudged the most accurate.

Exponential buckling measurements were performed in the SE to determine the temperature coefficient of reactivity for uniform heating of D_2O-cooled, 19-rod fuel clusters at 9.33- and 11.5-inch lattice pitches.

The SE buckling measurements were accompanied by foil activations to measure the detailed neutron reaction rates in the experimental lattices. Bare and cadmium-covered copper foils served to determine the thermal and epithermal neutron distributions in the lattices; Lu-Mn foil combinations served to determine the thermal neutron spectral indices. Similar measurements with ^{239}Pu-^{235}U foil combinations determined both spectral indices and the relative reaction rates of these two materials in the fuel. Measurements with uranium foils containing various concentrations of ^{235}U in ^{238}U served to determine resonance capture in ^{238}U, in terms of the cadmium ratio for the decay activity of ^{239}Np produced in the foils, and the relative numbers of ^{235}U and ^{238}U fissions in terms of the fission product activities produced in the foils.

The results of the experimental measurements were compared to calculations made with the HAMMER code[7], a one-dimensional, multienergy-group (54 fast, 30 thermal), integral-transport, lattice-cell calculation. This code is a "first principles" code in the sense that the calculations are made directly from the cell geometry and a cross section library based on measured differential cross sections with no arbitrary parameter adjustment. A concentric ring model preserving as much as possible of the original cluster geometry was devised to calculate the complex two-dimensional fuel clusters with this one-dimensional code.

The HAMMER buckling calculations matched the measurements quite well except for the 31-rod clusters at the 9.33-inch lattice pitch where systematic errors of up to 0.5 m^{-2} were noted. These discrepancies do not correlate with the type of fuel or coolant.

The temperature coefficient buckling measurements in the SE agreed closely with the computed values. Good agreement was also noted between the SE and PDP buckling measurements. The PDP buckling measurements and calculations are summarized in Figure 12, and the SE results are summarized in Figure 5.

The HAMMER calculations also gave generally good agreement with the measured foil activations. The agreement with the thermal neutron flux distributions was in general excellent, except for a tendency of the calculations to overestimate slightly the magnitude of the flux in the moderator when organic-cooled fuel clusters were used (Figures 13 and 14). The thermal neutron spectral index measurements were in somewhat less satisfactory agreement (Figures 15 and 16), although qualitatively they did follow the predicted behavior in all cases. The calculations of the fast fission effect were in close agreement with the measurements for the 19-rod clusters, but the measurements made on 31-rod clusters gave somewhat lower values than calculated. The main discrepancies noted in the resonance capture calculations were in the higher predicted values of resonance capture for the 31-rod clusters at the closer lattice pitches. These latter discrepancies were consistent with the buckling discrepancies observed for these same lattices, and hence the buckling errors are ascribed to errors in the resonance capture calculations.

It was concluded that the HAMMER code offers no difficulties in treating the burned-up fuel compositions and that it is fully adequate for survey calculations on D_2O power reactor lattices. However, some additional code development is indicated in the treatment of rod clusters and other geometrically complex fuel assemblies, in the treatment of thermal neutron energy exchanges, and in the treatment of resonance neutron capture at low moderator-to-fuel ratios.

DISCUSSION

DESCRIPTION OF THE FUEL ASSEMBLIES

Three sets of plutonium-bearing uranium oxide rods and a set of depleted uranium oxide rods were fabricated by Nuclear Fuel Services (NFS), Erwin, Tennessee. A matching set of natural UO_2 rods[1] had been fabricated earlier by General Electric, San Jose, California. The PuO_2-UO_2 powders were coprecipitated from the mixed nitrate solutions. Lots of 100 lb each were then formed from the dried oxide and blended for pellet formation. The pellets were sintered in a hydrogen furnace, centerless ground to a diameter of 0.500 ±0.002 inch, and loaded into 6063-T aluminum tubes. Samples of the oxide and the finished pellets from each blend were taken for chemical and isotopic analysis. The average "best" values of the chemical and isotopic analyses performed by the Analytical Chemistry Division of the Savannah River Laboratory (SRL) are given in Table I for each of the rod sets. A detailed discussion of the analyses is given in Appendix A. Table I also includes measured individual pellet and column average density values. The assays indicate that impurity levels in all samples are such as to contribute less thermal neutron absorption than the equivalent of 10 atomic ppm of natural boron (Table II). The uniformity of the plutonium distribution within the sintered pellets was tested by activation assays of minute samples from a crushed pellet. The measured plutonium agglomeration was well within acceptable limits. Details of this determination are given in Appendix B.

The standard types (A, B, C, and D) for fuel rods (Table I) are illustrated in Figure 1. The active fuel column length in these rods was 54 inches. Connectors at the ends of each rod permitted the rods to be joined together. The joints formed by the connectors introduced a filler of aluminum approximately 0.85 inch long between active sections of fuel. The Type E natural uranium fuel rod[1] was identical except for having an active length of 72 inches and a slightly different end fitting design.

Both 19- and 31-rod clusters (Figure 2) were used in the present experiments with the rods at 0.597-inch center-to-center triangular spacing. The rod-to-rod spacing was maintained by small bands of nylon placed along the individual rods.

The housing tubes used for the PDP buckling measurements were equipped with special pressure-tight top fittings so that, by remote valving procedures, D_2O could be admitted from the bottom of the assembly or expelled out the bottom by helium gas under pressure. Housings for both SE and PDP assemblies had

TABLE I

Assay of Fuel Pellets

Fuel Type	Density, g/cm³ (a) Pellet	Density, g/cm³ (a) Column	(Pu/U) (b)	Pu Isotope, wt % 239	Pu Isotope, wt % 240	Pu Isotope, wt % 241	Pu Isotope, wt % 242	U Isotope, wt % 234	U Isotope, wt % 235	U Isotope, wt % 236	U Isotope, wt % 238
A	10.421	10.23	0.00295	77.91	19.35	2.43	0.31	0.0012	0.302	0.0029	99.69
B	10.356	10.25	0.00259	93.00	6.17	0.79	0.04	0.0013	0.298	0.0032	99.69
C	10.380	10.26	0.00340	93.19	6.09	0.69	0.03	0.0012	0.301	0.0030	99.69
D (c)	10.403	10.38	-	-	-	-	-	0.0026	0.4979	0.0033	99.4962
E	-	10.39	-	-	-	-	-	0.0057	0.71	-	99.28

(a) NFS data.
(b) Pu/U fraction by weight - all isotopes included.
(c) Isotopic content of Type D fuel by ORNL; all others by SRL Analytical Chemistry Division.

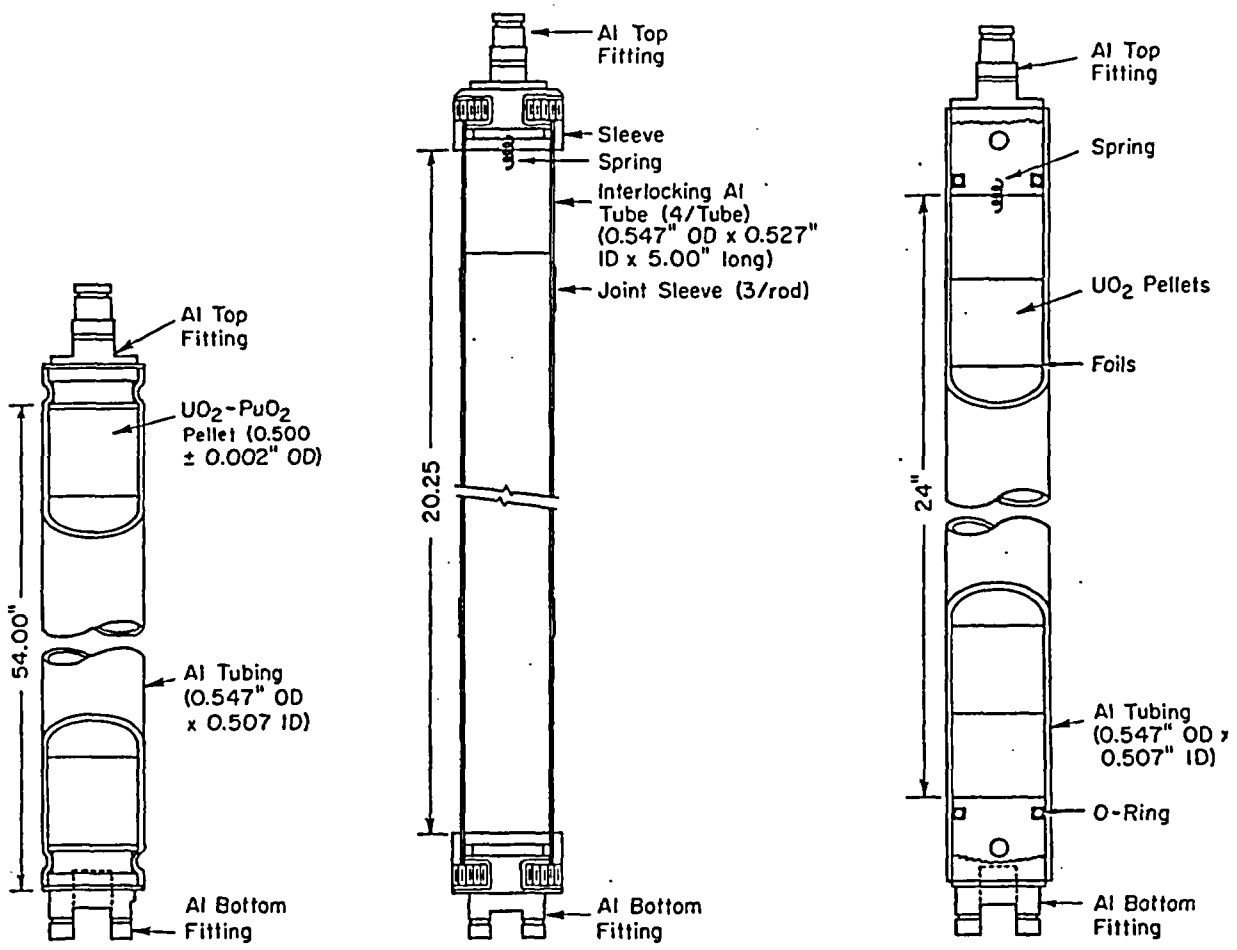

a. Sealed Full-Length Fuel Rod for Type A, B, C, D Fuel

b. Demountable Fuel Rod for Type A, B, C, D Fuel

c. Demountable Fuel Rod for Type E Fuel

FIG. 1 FUEL ROD TYPES

TABLE II

Impurity Analyses of PuO_2-UO_2 Fuels[a]

Fuel Type	Atomic ppm															
	Al	B	Ca	Cd	Cr	Cu	Fe	Mg	Mn	Mo	Na	Ni	Pb	Si	Sn	V
A	40	0.4	<10	<5	175	5	700	5	15	<10	50	20	<5	50	<10	<25
B	10	0.7	<10	<5	12	4	75	4	5	<10	100	15	<5	75	<10	<25
C	15	8	<10	<5	15	3	130	2	5	<10	75	20	<5	60	<10	<25

(a) Measurements performed by SRL Analytical Chemistry Division

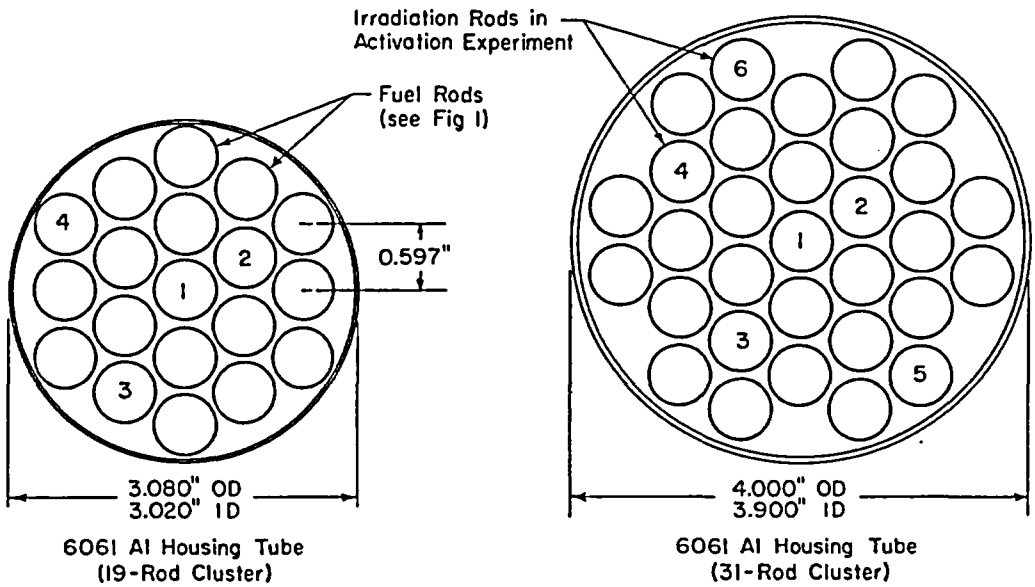

FIG. 2 FUEL CLUSTER ARRANGEMENT

plugs in the bottom to permit filling of the tubes with organic coolant material. These plugs also served to exclude D_2O for the air-cooled studies in the SE.

The organic coolant used was HB-40 (a liquid mixture of partially hydrogenated terphenyls, made by Monsanto). The room temperature density of HB-40 is ~1.00 g/cm^3, and its chemical composition is approximated by the molecular formula $C_{18}H_{22}$ (compared to $C_{18}H_{14}$ for ordinary terphenyl).

SPECIAL IRRADIATION RODS

Special rods were fabricated for the SE activation experiments. The Pu-bearing pellets were not handled bare because of the health hazard associated with plutonium metal. However, for the natural uranium measurements, the foils were introduced between the bare pellets.

Fuel Types A, B, C, and D Irradiation Rods

The foil irradiation rods for the fuel types A, B, C, and D measurements consisted of two 17-inch-long rods (shorter versions of the 54-inch rods of Figure 1a) fastened to a special middle rod, shown in Figure 1b. The middle rod contained four 5-inch-long fuel capsules clad with 0.005-inch aluminum (Figure 3). The foils were loaded in a machined recess that was an integral part of the top end cap for each capsule.

The faces of the fuel pellets at the ends of each irradiation capsule were polished to a smooth finish with square corners, and a thin spring was inserted near the center to provide reproducible geometry at the foil locations. The aluminum caps were glued to the thin-walled aluminum tube using Eastman 910 adhesive. Each cap was tested for straightness by rotating the assembled fuel capsule in a lathe while a dial micrometer was used to check the wobble. A maximum end-cap misalignment of 0.002 inch (measured on the circumference) was allowed in the irradiation capsules.

Natural Uranium Oxide Irradiation Rods (Type E)

The Type E irradiation rods used for experiments with organic coolants consisted of three sections of tubing with removable end fittings (Figure 1c). The sections were locked together to form a full-length rod, and the foils were placed in the middle rod section between individual fuel pellets. Full-length 6-ft rods with a window cut for access were used for the irradiations with D_2O and air as the cluster coolants.

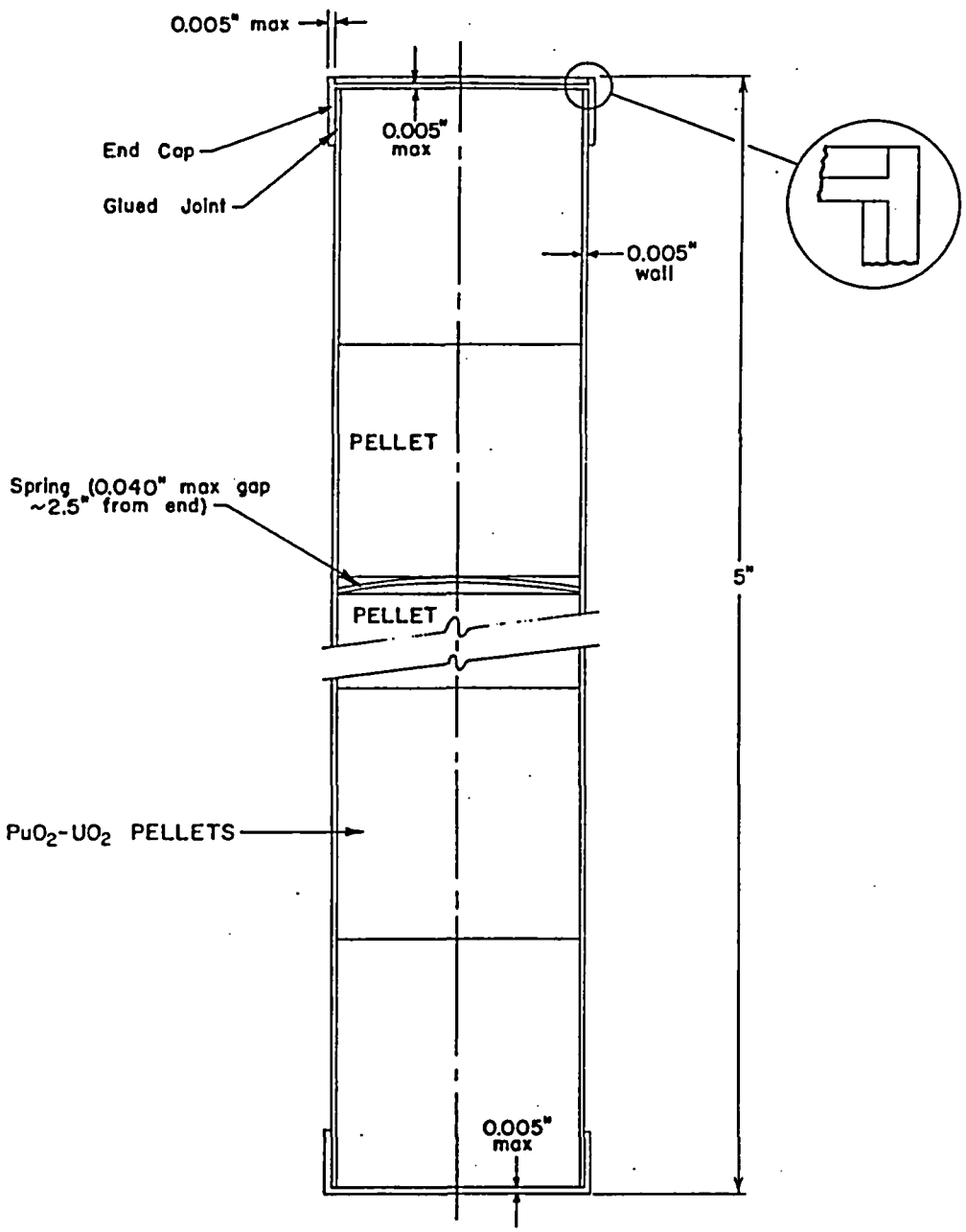

FIG. 3 THIN-WALLED UO_2-PuO_2 IRRADIATION CAPSULE

BUCKLING MEASUREMENTS

The PDP Facility

The Process Development Pile (PDP)[2] is a critical facility for reactor physics studies at power levels below 10 kw. Moderated by heavy water, it is designed for maximum experimental flexibility and can accommodate a wide variety of lattice components in almost any desired configuration. The PDP tank is 16 feet 2-3/4 inches in diameter with a height of 15 feet 6 inches. A system of grid beams at a center-to-center spacing of 6.06 inches is used for top support of the lattice components. The control system besides providing a variety of safety, shutdown, and control rods permits the moderator level to be adjusted and maintained to within ±0.002 cm. Vernier water level control is maintained by balancing a variable flow input against a small fluid drain. Absolute water heights may be measured to an accuracy of ±0.1 cm and relative water heights to ±0.001 cm. Pile power is monitored by boron-lined ionization chambers connected to picoammeters. Final criticality is ascertained with differential pile power instrumentation.

Lattice Bucklings by Substitution

Buckling measurements were made in the PDP by the substitution method. Host lattices of natural UO_2 (Type E) rod clusters were selected whose nuclear properties approximated those of the test lattice. Fuel assemblies for the host lattices consisted of 19- or 31-rod clusters corresponding to the cluster size and lattice pitch of the test lattice. Host fuel assemblies differed from test assemblies in four respects: (1) the host assemblies had a center-to-center rod spacing of 0.650 inch rather than the 0.597 inch of the test assemblies; (2) the host assemblies were devoid of housing tubes; (3) the host assemblies used only natural UO_2 fuel; and (4) the host assemblies used only D_2O coolant. Material bucklings for the host lattices were determined by measurement of axial and radial neutron flux profiles from bare and cadmium-covered gold pin activations. The foil activations were least squares fitted to the fundamental mode functions [$J_0(B_R r)$ for the radial and $\sin(B_Z z)$ for the axial].

A summary description of the host lattice loadings and bucklings is given in Table III. The host lattices were used in reduced core loadings in order to eliminate the low critical water heights required by a full load. A typical loading is shown in Figure 4a. The radial region outside the fuel was poisoned with a uniform distribution of Li-Al poison rods. These rods defined a boundary for the core with characteristics resembling

TABLE III

PDP Reference Lattice Data[a]

attice No. 1

Loading: 85 19-rod clusters at 9.33-inch triangular pitch.

$B_z^2 = 1.909\ m^{-2}$

$B_r^2 = 3.69\ m^{-2}$

$B_m^2 = 5.60 \pm 0.16\ m^{-2}$

Moderator, 99.565 mol % D_2O, 21.27°C

Lattice No. 2

Loading: 85 31-rod clusters at 12.12-inch triangular pitch.

$B_z^2 = 2.588\ m^{-2}$

$B_r^2 = 2.14\ m^{-2}$

$B_m^2 = 4.72 \pm 0.14\ m^{-2}$

Moderator, 99.540 mol % D_2O, 20.83°C

Lattice No. 3

Loading: 121 31-rod clusters at 9.33-inch triangular pitch.

$B_z^2 = 2.849\ m^{-2}$

$B_r^2 = 2.44\ m^{-2}$

$B_m^2 = 5.29 \pm 0.16\ m^{-2}$

Moderator, 99.507 mol % D_2O, 21.48°C

(a) The buckling values are for the reference lattices with control rod guide tubes in place, i.e., as in the substitution measurements.

a vacuum boundary rather than those of a large reflector, and thus minimized errors in buckling measurements of the host lattice and the subsequent substitution lattices.

The central seven cells of the host lattice served as the substitution region. Figure 4b shows different methods for substitution of one, two, three, or seven test assemblies into this region.

Three methods of analyses were employed to infer test lattice bucklings from the critical water height changes resulting from the substitutions. Two of these methods, notably the Persson successive substitution method[5] and the two energy-group diffusion theory method, have been used previously at SRL, and have been described in detail[4]. The Persson method is based on solution of the one-group perturbation equations. The mixed lattice is divided into subcells of three types: host, test, and mixed. It is assumed that a single

buckling is applicable to all subcells of a single type and that the material buckling of the composite reactor, given in terms of critical dimensions, can be expressed as the statistically weighted sum of the bucklings of the three lattice regions. Added terms dependent on flux derivatives are included to account for differences in diffusion coefficients between regions. Neglecting differences in diffusion coefficients, one has for the overall reactor buckling

$$B^2 = W_1B_1^2 + W_2B_2^2 + W_3B_3^2 \qquad (1)$$

where B_1^2, B_2^2, and B_3^2 are respectively the host lattice buckling, the mixed-lattice buckling, and the test lattice buckling and the W's are the respective statistical weights. The three bucklings can be obtained by simultaneous solution of three linear independent equations of the form of Equation 1. These equations can readily be formulated by three different loadings with different ratios of statistical weights. One of these loadings is normally the one-region host lattice ($W_1 = 1$, $W_2 = W_3 = 0$). In order to utilize a simple least squares method for treating more than three cases of a single system, Persson recasts Equation 1 into the linear form

$$\left(\frac{B^2 - B_1^2}{W_3 + W_2/2}\right) = \delta B^2 \left(\frac{W_2}{W_3 + W_2/2}\right) + (B_3^2 - B_1^2) \qquad (2)$$

where

$$\delta B^2 = B_2^2 - \frac{B_3^2 - B_1^2}{2}$$

and the identity $W_1^2 + W_2^2 + W_3^2 = 1$ has been used. Equation 2 is of the form $y = ax + b$ with the identification in the order listed. At $x = 0$ ($W_2 = 0$, $W_3 = 1$), the y intercept of this equation is the difference in material buckling of the test and host lattices; the slope is δB^2.

The extension of Equation 2 to cases involving anisotropic diffusion and regional differences in diffusion coefficient is straightforward but tedious.[4,5] The result is that an equation of the form $y = ax + b$ is again obtained, where a and b are defined exactly as in Equation 2, but y and x are much more complicated quantities involving ratios of diffusion coefficients and weighting functions based on the derivative of the flux shape. The $x = 0$ intercept also requires a small computed correction to give the difference in test and host lattice bucklings.

Radial statistical weight functions are computed from the product of the perturbed flux and the J_0 unperturbed flux. A one-group, two-region computation is used to derive the perturbed flux for each substituted lattice from the change in critical

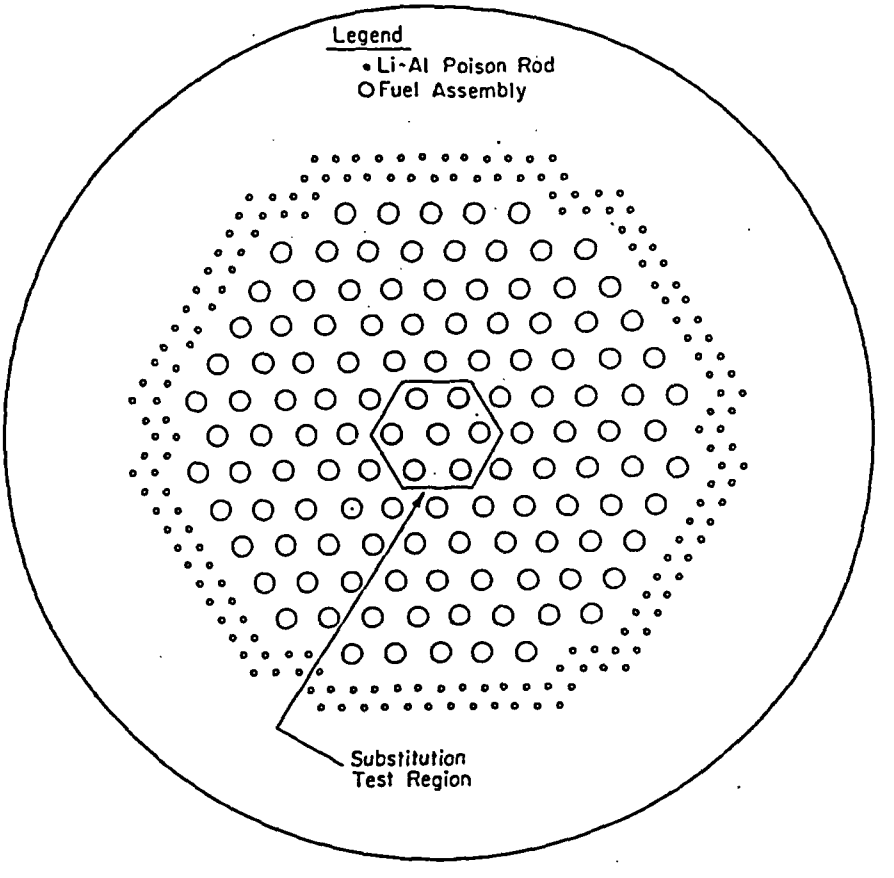

a. Full Lattice

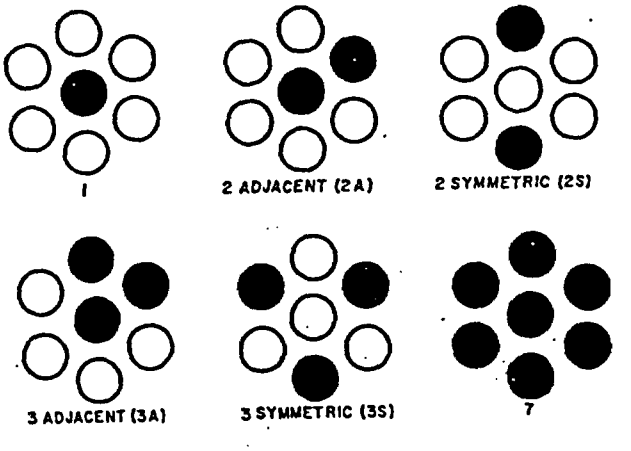

b. Test Region (Solid Circles are Substituted Test Assemblies)

FIG. 4 TYPICAL LOADING OF PDP FOR SUBSTITUTION BUCKLING MEASUREMENTS

water height. Statistical weights are computed by a numerical integration over the Persson cells, which are further subdivided for this integration.

The computation of the perturbed flux and the assignment of statistical weights are performed in a single computer code. The method is described in detail in DP-832.[4]

The required data, other than the critical dimensions and details of the loading, are the diffusion coefficients in the different lattices. These were derived from the HAMMER computations, which are detailed in a later section. For the gas-cooled lattices, anisotropic effects were included by measurement and calculation. The difference between the diffusion coefficients of the moderator and of the lattice in the axial direction was measured by the method outlined in DP-832. The effect in the radial direction was included by means of Benoist's method[8]. A weighted average of the slow and fast diffusion coefficients was obtained by

$$D_{eff} = \frac{L^2 D_S + \tau D_F}{L^2 + \tau}$$

where D_S and D_F are the slow and fast group diffusion coefficients, and L^2 and τ are the slow and fast migration areas.

The second method, direct use of two-group diffusion theory, could be applied only to those loadings which formed a reactor-centered, nearly cylindrical, test region. The one-rod, seven-rod, and perhaps the three-adjacent-rod substitution cases of Figure 4b satisfy this requirement. For these analyses, an input of the critical dimensions, the host lattice bucklings, the effective radius of the test region, slow and fast diffusion coefficients, slow and fast migration areas, and resonance escape probabilities for test and host lattices were required. These data in the two-group critical equation uniquely specify the material buckling of the test lattice. The method has been detailed in earlier reports.[4,9]

The third method involved use of the HERESY code for source-sin heterogeneous lattice calculations.[10] The HERESY code treats all fuel rods as idealized line sources of fast neutrons and as line sink of monoenergetic resonance neutrons and of monoenergetic thermal neutrons embedded in a uniform sea of moderating material. For the present application, required input data included a parameter definin the thermal neutron absorption and the energy at which resonance absorption takes place. These values were derived from the HAMMER computations except for the effective resonance energy, which was derived from earlier experiments. These data along with the physical

description of the lattice grid and the moderator properties permitted the code to perform a criticality search on η (or equivalently k_∞) or the lattice dimensions (geometric buckling) depending on which is left unspecified. The method in outline form follows:

1. Critical dimensions of the host lattice alone are determined.

2. Critical dimensions and the other required parameters are inserted into the HERESY code to determine a consistent η value for the host lattice.

3. The altered critical dimensions of the substituted load are measured (change in critical water height).

4. The new critical dimensions are put into a HERESY computation, and a search is made for η of the substituted test assemblies.

5. The newly derived value of η and the previously used test lattice parameters are put into a new HERESY problem consisting of a full load of the test fuel, and a search is made for the critical dimensions. The critical dimensions then give the desired test region material buckling.

A summary of all the measured test lattice bucklings is given in Table IV. A more detailed description of the measurements and analytical results is given in Appendix C.

TABLE IV

Material Bucklings from Analysis of PDP Substitutions

Coolant	Buckling, m^{-2}(a)				
	Fuel A	Fuel B	Fuel C	Fuel D	Fuel E
	Lattice(b) 1, 19-rod cluster, 9.33-inch pitch				
D_2O	4.39 ±0.15	5.24 ±0.15	7.17 ±0.15	0.23 ±0.30	5.34 ±0.15
HB-40(c)	1.50 ±0.25	2.18 ±0.25	(d)	-2.52 ±0.70	(d)
Void	4.56 ±0.20	5.32 ±0.15	7.26 ±0.15	0.18 ±0.60	5.46 ±0.15
	Lattice(b) 2, 31-rod cluster, 12.12-inch pitch				
D_2O	3.56 ±0.20	4.29 ±0.15	6.00 ±0.15	0.19 ±0.30	4.41 ±0.15
HB-40(c)	0.66 ±0.35	1.06 ±0.15	2.84 ±0.20	-3.04 ±0.70	1.12 ±0.35
Void	3.92 ±0.20	4.62 ±0.15	6.35 ±0.15	0.21 ±0.40	4.71 ±0.15
	Lattice(b) 3, 31-rod cluster, 9.33-inch pitch				
D_2O	3.84 ±0.20	5.01 ±0.15	7.26 ±0.15	-1.15 ±0.35	5.02 ±0.15
HB-40(c)	0.86 ±0.40	2.07 ±0.30	4.57 ±0.20	-4.75 ±0.80	1.79 ±0.35
Void	3.88 ±0.35	5.03 ±0.20	7.19 ±0.20	-0.64 ±0.40	5.01 ±0.15

(a) For fuel type, see Table I.
(b) For reference lattice data, see Table III.
(c) Monsanto Company, St. Louis, Missouri.
(d) No experiment performed.

TEMPERATURE COEFFICIENT MEASUREMENTS

The SE-SP Facility

The Subcritical Experiment[3] (SE) is an upright cylindrical tank in which exponential experiments are conducted on subcritical lattice arrays. D_2O was used as the SE moderator in the present experiments. The fuel loading, the lattice spacing, and the filling of fuel coolant channels were varied.

The 5-ft diameter and 7-ft high tank is made of aluminum with a cadmium wrapping and is centered immediately above the SP[3] reactor, which serves as a neutron source. The SP is a 5-ft cube of graphite with a water-cooled core of ^{235}U-Al fuel. The facilities are coupled through a cylindrical graphite pedestal, which serves to minimize spatial harmonics in the cylindrical SE from the cubical source reactor. The background effect of extraneous neutron sources such as fast neutrons from the reactor and photoneutrons from deuterium in the moderator is determined by interposing a cadmium shutter between the pedestal and the SE tank. Background-corrected axial flux profiles are then obtained as the difference between shutter-out and shutter-in runs. All axial traverses are obtained with a small, boron-lined, gamma-compensated ion chamber that is driven at a constant speed. Digitized current readings are transferred to computer data cards at 2-cm axial intervals. These readings are fitted numerically by a least squares method to analytic functions describing the axial flux shape to determine the axial relaxation length, κ. The material buckling is obtained by the relation

$$B_m^2 = B_R^2 - \kappa^2$$

where the room temperature radial buckling, B_R^2, was taken to be 9.25 m^{-2} at 20°C for all the lattices studied in these experiments.

Buckling Measurements in the SE

Exponential buckling measurements were made in the SE on 19-rod clusters of Type B fuel at lattice pitches of 9.33 inches triangular and 11.5 inches square to determine the temperature coefficients for uniform heating of these lattices. For these measurements, no housing tubes were used around the fuel clusters. The moderator purity was 99.52 mol % D_2O.

The moderator was heated by immersion resistance heating elements placed on the bottom of the SE tank. These elements remained in place during the experimental buckling determinations. Previous experiments had shown their effect on the measured bucklings to be negligible.

The axial bucklings at the temperatures indicated in Figure 5 were determined by least squares fitting the points of the measured axial flux shape to a hyperbolic sine. The radial buckling of 9.25 m^{-2} at 20°C was assumed to decrease by 0.01 $m^{-2}/°C$. A small error in the assumed radial buckling was introduced by the effect of the heater electrical lines located near the tank wall, but the slope of the points (or linear temperature coefficient of reactivity) would be unaffected.

If the four measured bucklings of each pitch are fitted to a straight line, the temperature coefficients thus inferred are 0.0052 $m^{-2}/°C$ for the 9.33-inch triangular pitch and 0.0011 $m^{-2}/°C$ for the 11.4-inch square pitch.

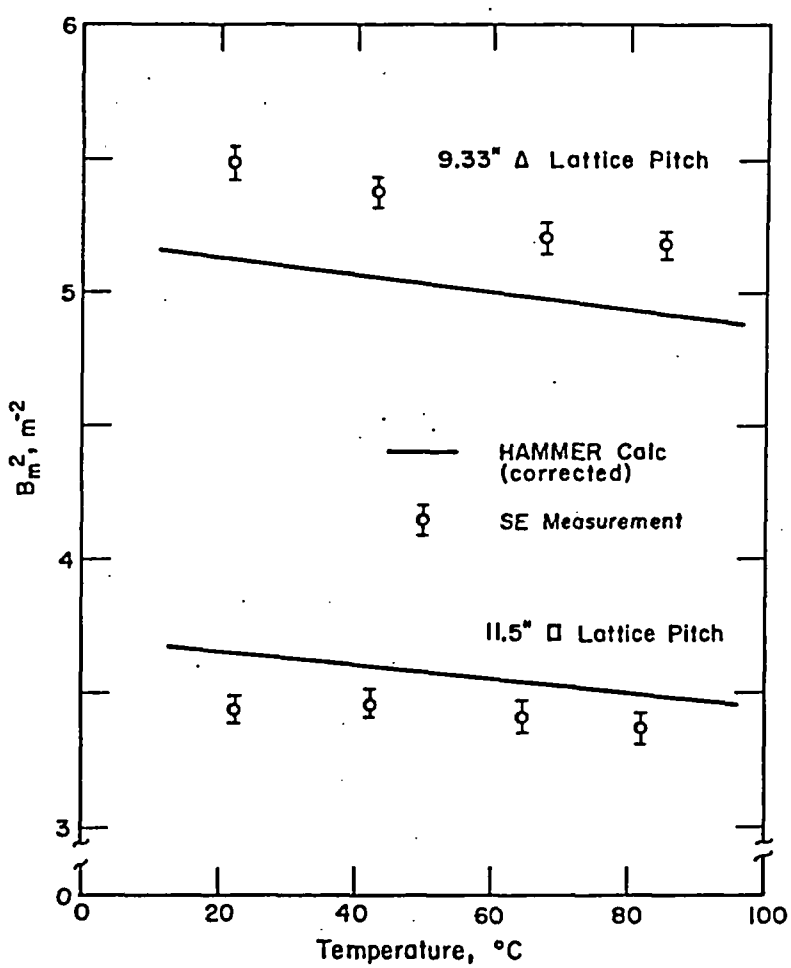

FIG. 5 TEMPERATURE COEFFICIENT OF THE LATTICE BUCKLING
19-Rod Clusters Type B Fuel, No Housings
99.52 mol % D_2O Coolant and Moderator

ACTIVATION EXPERIMENTS

Foil Loadings

A total of nine different materials were used for foil activations. A brief description of the foil types and counting methods is given in Table V. Individual foils were loaded into the special irradiation rods as indicated in Figure 6 for fuel Types A, B, and C and in Figure 7 for Type E fuel. The perturbing effect of cadmium pillboxes was minimized in the Pu-bearing rods by making two separate runs for each lattice, one of which was completely devoid of cadmium. In the Type E fuel the cadmium pillboxes were located outside the range of interaction.

The four to six irradiation rods used in each run were combined with normal fuel rods of the same type and positioned as shown in Figure 2. The special irradiation assembly was then loaded into the center of the SE, as indicated in Figure 8, surrounded by six identical test fuel assemblies (except for the detector foils). The surrounding host lattice consisted of 19-rod clusters of Type E fuel with no housing tubes and a center-to-center rod spacing of 0.650 inch.

Bare and cadmium-covered Lu-Mn-Al foils were suspended in the moderator perpendicularly from the central assembly along a line directed midway between adjacent fuel assemblies. The foils were held between two lightweight strips of polyester tape, which were stretched across a rectangular loop of aluminum wire.

As indicated in Figure 8, two interstitial foil holders were included in each run. One of these held foils of manganese, tungsten, indium, lutetium, and copper, which served as intracell "known-spectrum" reference foils. The second served as a monitor for differences in axial fluxes at the different foil elevations. Bare copper foils were positioned on this holder at precisely the same elevations as the foils within the irradiation assembly.

A well-thermalized position for activating reference foils in a thermal neutron flux was established 10 inches inside the graphite thermal column of the SP (Figure 9a). The reference foils were mounted at a common radius on an aluminum spinner disc that was rotated during the exposure. Relative exposure histories for the reference and sample foils were identical in each run since the SP supplied irradiation neutrons simultaneously to the SE and thermal column. The measured cadmium ratio (0.032-inch Cd) for thin (2-mil) gold at the thermal reference position was approximately 2800, which gives an equivalent 1/v cadmium ratio of 3×10^4.

TABLE V

Description of Foils and Gamma Counting Procedures

Detector	Activity	Half-Life	Foil Description: Active wt %	Foil Description: Material	Foil Description: Thickness, inch	Foil Description: Diameter, inch	Counter Bias, kev	Counting Interval after Irradiation
^{115}In (a)	^{116m}In	54 min	1	Al-In	0.005	0.500	100	1- 4 hr
^{186}W	^{187}W	24 hr	-	W	0.002	0.500	40	18-26 hr
^{63}Cu	^{64}Cu	12.9 hr	-	Cu	0.005	0.500	400	4-18 hr
^{55}Mn (a)	^{56}Mn	2.58 hr	10	Lu-Al-Mn	0.010	0.500	500	1- 6 hr
^{176}Lu (a)	^{177}Lu	6.8 days	5	Mn-Al-Lu	0.010	0.500	35	2- 4 days
^{239}Pu (a)	FP	-	3.1	Pu-Al	0.005	0.500	500	2-10 hr
^{235}U	FP	-	5	U-Al	0.002	0.500	500	2-10 hr
Nat U	FP ^{239}Np	- 2.35 days	-	U	0.006	0.500	500 90-116 window	2-10 hr 2- 4 days
Depl U	FP ^{239}Np	- 2.35 days	-	U	0.006	0.500	500 90-116 window	2-10 hr 2- 4 days

(a) These foils were loaned to SRL by AECL.

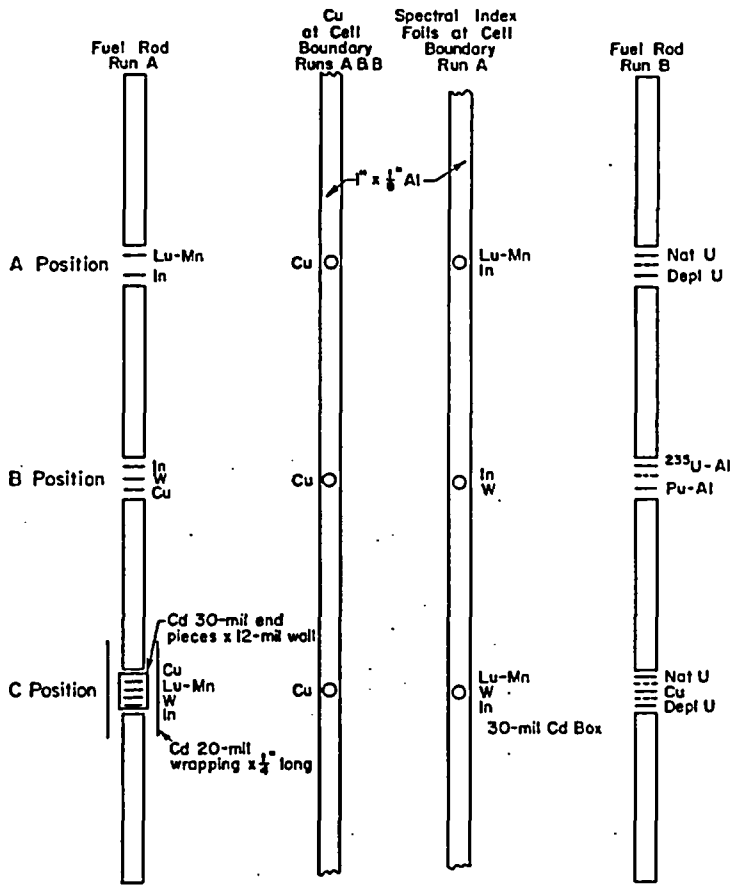

FIG. 6 SCHEMATIC OF FOIL LOADING IN UO_2-PuO_2 LATTICE MEASUREMENTS

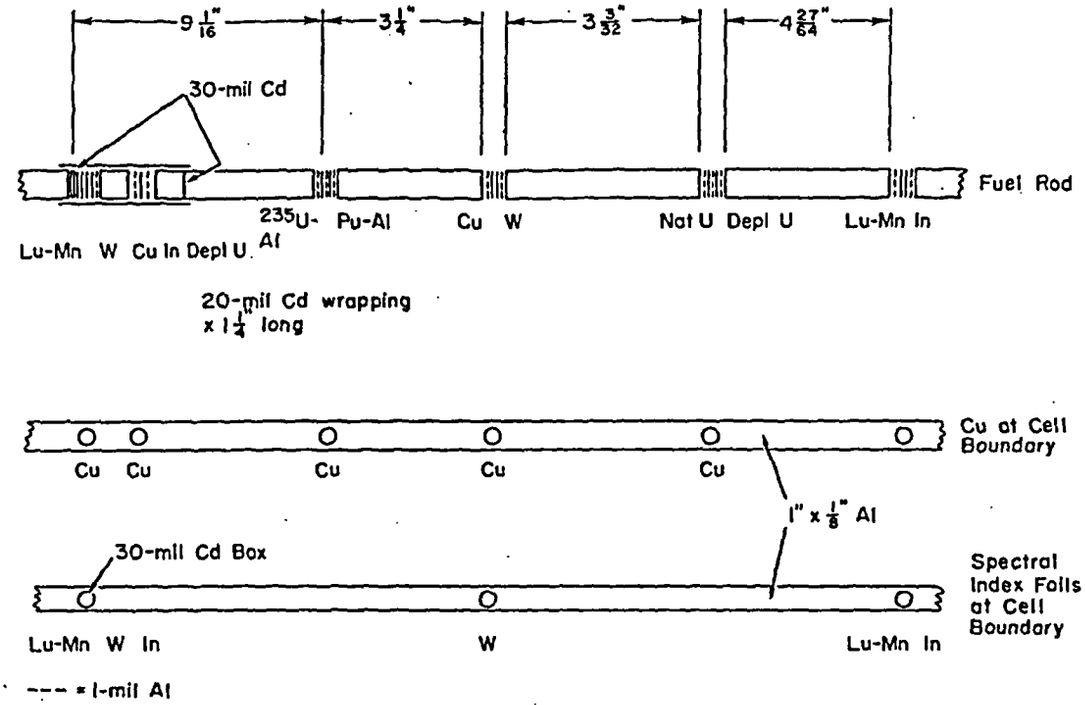

FIG. 7 SCHEMATIC OF TYPICAL FOIL LOADING IN NATURAL URANIUM (TYPE E) LATTICES

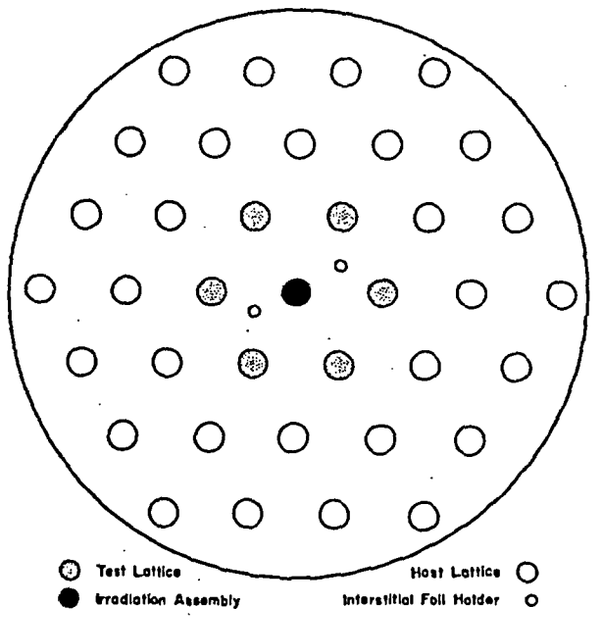

FIG. 8 SE FACE MAP FOR IRRADIATION EXPERIMENTS
(9.33" Δ Lattice Pitch)

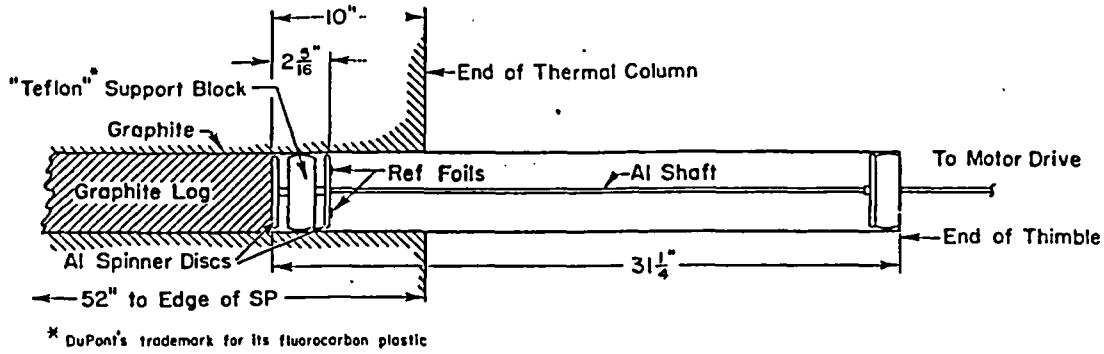

(a) Thermal Neutron Reference

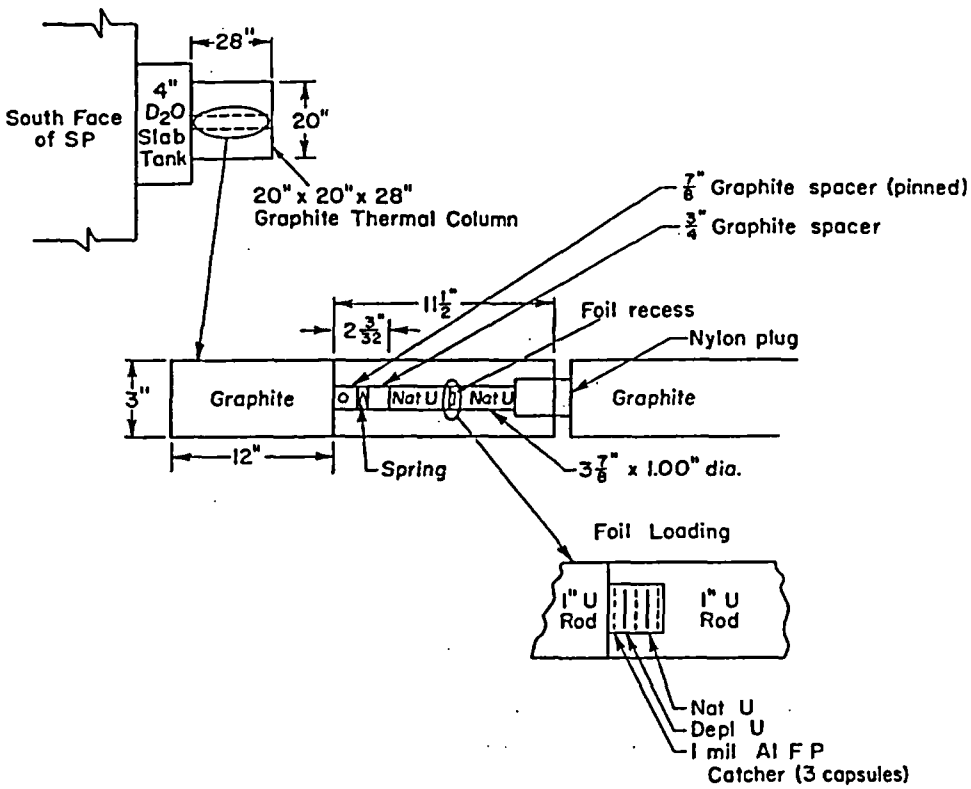

(b) Fast Fission Reference

FIG. 9 REFERENCE FLUX POSITIONS FOR ACTIVATION EXPERIMENTS

Resonance Capture

Depleted and natural uranium metal foils were used to determine ^{238}U neutron capture in the oxide rods. The total amount of filler material at the foil position (natural and depleted uranium, copper, aluminum catcher foils, and aluminum end caps) was selected to approximate the average macroscopic thermal absorption cross section and the ^{238}U atom density within the oxide.

The relative numbers of ^{238}U captures were measured by counting the 2.3-day activity of $^{239}Np \rightarrow {}^{239}Pu$. The gamma activities and the K_α and K_β X-rays were counted by sodium-iodide (thallium activated) scintillators, biased to accept energies in the interval from 90 to 116 kev. A simultaneous count was made on each foil at an integral bias of 500 kev. This latter bias excludes all capture decay and is a monitor of fission product activity. Counts were made from 2 to 5 days after the irradiation to minimize the background fission product activity relative to the desired capture activity. After counting, the normal background corrections (including spontaneous decay) were made. Corrections for small differences in weight and γ-ray attenuation factors due to small differences in foil thicknesses were also included. The attenuation factors were determined in an auxiliary experiment using different thicknesses of ^{238}U absorber and irradiated ^{238}U as a source. Foil thicknesses were kept small and counter geometries were maintained with small acceptance angles to minimize foil edge effects in the γ attenuation.

Extrapolation to zero fission product activity was obtained by combining the data from the paired natural and depleted uranium foils. A slight departure from the normal method exploited the properties of the flux at the thermal reference position. Natural and depleted uranium foils from this position alone were used to obtain the relation between fission product activity in the monitor channel (> 500 kev) and the activity due to fission products in the channel defined by the 90 to 116 kev window. The channel activities needed to obtain this ratio were obtained very simply for the thermal reference foils by subtracting the specific activity of the depleted foil expressed as the counting rate per ^{238}U atom from that of the natural uranium foil. This ratio can be obtained far more accurately in the thermal column than in the lattice cell for two reasons. First, in a purely thermal flux the desired fission product activity is larger relative to the ^{239}Np activity, which for this determination is a nuisance background. Second, this background activity from a nonresonant thermal flux is quite insensitive to the minor geometrical imperfections common to the foils. An added advantage of this method is that the activities of natural and depleted foils in the UO_2 rods are weighted equally whereas in the conventional method undue weight is given to the depleted foil. (As a corollary, this method makes

redundant the use of two foil materials in each rod.) No systematic differences were noted in ^{238}U activities deduced from the two foil types. Two assumptions implicit in this method are that the energy distribution of gamma and beta rays from ^{238}U fission is closely that from ^{235}U fission and that the ^{235}U distribution does not depend strongly on the energy of the fissioning neutrons. These assumptions cannot be verified without chemical separation techniques since no direct counting method is available for obtaining fission capture in ^{238}U without some radiative capture.

Because no cadmium-covered ^{238}U detectors were used, the cadmium ratio (or equivalently $\rho \equiv [(\text{Cd ratio} - 1)^{238}]^{-1}$ had to be derived indirectly. This was accomplished by noting that the capture cross sections of both ^{238}U and Cu (or Mn) follow the 1/v law closely in the subcadmium region. Thus the subcadmium copper activity can be used to represent the subcadmium ^{238}U activity in the fuel if the two detector foils are normalized in a thermal flux (thermal column). A similar normalization to ^{235}U and/or ^{239}Pu in lieu of the copper (a technique long employed at Chalk River) allows a direct interpretation of the measurements in terms of conversion ratios rather than of ρ.

The ρ values for the cell were obtained from the epicadmium and subcadmium activities separately averaged over the 19 or 31 rods of the cluster. The values are listed in Table VI. The measured ratio of ^{238}U capture to ^{235}U fission, C*, is also included in this table.

TABLE VI

Resonance Capture and Fast Fission in Clusters of Uranium Oxide Rods

Cluster[d] Type	Coolant	D_2O Purity, mol %	ρ HAMMER Cylind	ρ HAMMER Corr	ρ Expt Cu	ρ Expt Mn	ρ Expt Avg	δ_o[a] HAMMER	δ_o[a] Expt	δ[b] HAMMER	C*[c] HAMMER Cylind	C*[c] HAMMER Corr	C*[c] Expt Nat-Depl	C*[c] Expt ^{235}U-Al
19-A	D_2O	99.57	.373	.390	.368	-	.368	.0468	.049	.0525	2.085	2.110	2.18	2.21
19-B	HB-40	99.48	.348	.372	.337	-	.337	.0467	.048	.0503	2.072	2.106	2.10	2.12
19-C	HB-40	99.65	.410	.438	.437	-	.437	.0550	.056	.0505	2.150	2.193	2.18	2.21
19-C	D_2O	99.66	.436	.456	.400	-	.400	.0556	.056	.0507	2.203	2.234	2.17	2.23
19-C	Air	99.66	.404	.417	.391	-	.391	.0568	.054	.0521	2.166	2.186	-	-
19-E	HB-40	99.64	.339	.362	.366	.304	.335	.0456	.045	.0456	.8707	.8722	.863	.805
19-E	D_2O	99.65	.362	.380	.357	.375	.366	.0458	.041	.0458	.8882	.8893	.913	-
19-E	Air	99.66	.336	.347	.341	.353	.347	.0471	.050	.0471	.8740	.8812	.870	.763
31-C	D_2O	99.63	.694	.691	.655	-	.655	.0696	.060	.0623	2.582	2.575	2.53	2.59
31-C	HB-40	99.61	.588	.585	.571	-	.571	.0691	.065	.0618	2.427	2.427	2.45	2.42
31-E	D_2O	99.63	.563	.560	.500	.520	.510	.0563	-	.0563	1.009	1.004	.988	-
31-E	HB-40	99.59	.476	.473	.423	.433	.428	.0559	-	.0559	.958	.954	.942	.835

(a) δ_o is 238/235 fission ratio in natural uranium foils.
(b) δ is the ratio of ^{238}U + ^{240}Pu fissions to ^{235}U + ^{239}Pu + ^{241}Pu fissions in the fuel.
(c) C* is the ratio of total ^{238}U captures to ^{235}U fissions in fuel cluster.
(d) See Table I and Figure 2.

Fast Fission Effect

The same paired natural and depleted uranium foils used for the resonance capture measurements were also used to determine the fast fission effect. The ratio δ_0 of ^{238}U fast fission to ^{235}U total fission was obtained by counting the paired foils at an integral bias of 500 kev at a time interval from 4 to 16 hours following the irradiation. Because of conflicting demands for counting equipment, it was impossible to standardize counting conditions with regard to such factors as geometry, bias, and time (conditions essential in the normal methods of determining δ_0). Instead, all measurements were normalized to measurements made in a fixed reference position (with a fixed "known" δ_0 value). This reference position consisted of a single 1-inch diameter, 8-inch-long slug of natural uranium metal embedded in graphite. Fully thermalized neutrons from the SP were fed to a special assembly containing the slug and graphite. The arrangement is shown schematically in Figure 9b. The reference foils within the "ϵ reference" rod were a pair of natural and depleted uranium foils identical to those in the lattice. These foils were placed in a shallow circular recess milled into the center face of one of the two 4-inch-long segments making up the slug.

The relative ^{235}U contents of the depleted and natural uranium foils were assayed by activation of the foils in a fully thermalized neutron flux, thus eliminating fission product activity from fast fission in ^{238}U. This method of normalization gives an effective concentration which is the true concentration multiplied by the fission product retention fraction. This retention probability is closely the same for all of the natural foils (0.005 mil thick) and depleted foils (0.006 mil thick) separately. The effective ^{235}U content of the depleted foils was determined to be 0.0446 wt % compared to a nominal 0.035 wt %. With a known fixed value of δ_0 in the reference lattice, it is easy to recalibrate for P(t), the quantity which relates the ratio of fission product activities to the true fission ratio for the two isotopes by maintaining the same neutron exposure conditions and counting times for reference and lattice foils. The values quoted in this report are based on a value of $\delta_0 = 0.070$ for the 1/2-inch foils at the center of the 1-inch-diameter rod. This value was obtained by a comparison of the natural and enriched uranium foil activities at the irradiation position in the center of the 1-inch-diameter slug to the activities of similar 1-inch-diameter foils covering the full slug cross section. The reference value of δ_0 for the 1-inch foils was taken to be 0.053. The quoted values of δ_0 can be altered by a simple

ratio of reference values, if it is desired to change the 0.053 value assigned to δ_o for the 1-inch-diameter reference rod.

The fast fission factor was not completely determined by the experimental method used because the fission events that occur in the plutonium isotopes were not considered. The values of δ_o quoted in Table VI are simply the cluster average of ^{238}U to ^{235}U fissions for natural uranium detector foils.

Neutron Spectral Index

Neutron spectral indices were measured by paired foils of Mn-Lu and of ^{239}Pu-^{235}U. The latter results are of particular interest because they measure lattice reaction rates as well as the spectral indices.

The Lu-Mn foils were provided by the Chalk River Laboratories and consisted of composite foils containing both Mn and Lu in an Al matrix. These combination foils have the advantage of minimizing dependence on geometrical placement (except insofar as Lu and Mn are not distributed uniformly within the foil). The short-lived Mn activations were readily separated from the Lu activations by maintaining an integral bias in the scintillation counting above that of the low energy Lu activity. Further, the long-lived ^{177}Lu activations were readily separated from the short-lived ^{176}Lu and Mn activations by delaying the counting for several days. Because of the relatively low activities of the Lu, it was necessary to count each foil for a total time of about one hour. A bias of 30 kev was used. Background was a special concern with the low count rate. It was minimized by using thin (0.2-inch) NaI(Tl) crystals. Assays of Mn and Lu separately in each foil were obtained by activation in a uniform thermal flux (a spinner externnal to the SP).

All activations, including Lu and Mn, were normalized to unity at the thermal reference position. The ratios of Lu-to-Mn subcadmium activities in the fuel then give the normalized spectral indices. These indices are somewhat loosely labeled $[g_{Lu}/g_{1/v}]$ because of the similarity to the Westcott "g" factors. They are not directly comparable to the Westcott values, however, because of the difference in normalization and the difference in the neutron energy range considered. The measured ratios are directly

comparable to quantities computed by HAMMER. The exact equivalent ratio from HAMMER is

$$g_{Lu}/g_{1/v} = \left[\frac{\sigma_{Lu}}{\sigma_{1/v}}\right]^{\text{Lattice}}_{\text{HAMMER}} \Bigg/ \left[\frac{\sigma_{Lu}}{\sigma_{1/v}}\right]^{\text{Th Ref}}_{\text{HAMMER}}$$

where the cross sections are averaged by the THERMOS section of HAMMER over the appropriate flux spectra in the energy interval from zero to 0.625 ev. The HAMMER library gives for a purely Maxwellian thermal flux at 20°C an average value of σ_{Lu} = 3080.6 barns for ^{176}Lu and a value (except for numerical round-off) of $\sqrt{\pi/4}$ for $\sigma_{1/v}$ normalized at 2200 m/sec.

Intracell Flux Profiles

The intracell flux profiles were obtained from the subcadmium manganese activation of the same Mn-Lu-Al foils used for the spectral index measurements. The foils in the moderator were placed at identically the same vertical position as the associated foils in the fuel rods, thus eliminating any height correction. A single radial line was used for these foils. Corrections for radial leakage were made to the experimental data. These corrections consisted of dividing all data by $J_o(B_R r)$, where B_R^2 is the radial buckling of the SE and r is the radial position of the individual foils.

A summary of all foil activations, except for those used to derive δ_o, is given in Tables VII through XVIII. All activations have been corrected for axial and radial flux differences and include the normal background, decay, deadtime, γ attenuation, and foil weight corrections. In addition all activations have been normalized to the subcadmium activations at the thermal column reference positions. (It should be noted that this normalization has no simple interpretation in intercomparing the different lattices.)

In these tables no correction has been made for perturbations caused by the foil materials or by the gap introduced by the aluminum end caps of the Pu-bearing rods. Also the subcadmium activities are obtained by simply subtracting the appropriate cadmium-covered activity from that of the bare foils, and the cadmium ratio is simply the ratio of the two activities; i.e. no correction has been applied for cadmium shielding of the resonances.

TABLE VII

Foil Activations for 19-Rod Clusters of Type A Fuel with D_2O Coolant (99.57 mol % D_2O Coolant and Moderator)

	Fuel Rod Position (see Figure 2)						
	1	2	3	4	5	6	Edge of Cell
Run B							
Total ^{238}U capture	2.483	2.631	3.036	3.244	-	-	-
	2.238	2.614	3.008	3.231	-	-	-
	2.520	2.702	3.146	3.342	-	-	-
	2.510	2.642	3.094	3.291	-	-	-
Subcadmium ^{63}Cu	1.822	1.950	2.254	2.397	-	-	-
Total ^{235}U fission	1.778	1.904	2.203	2.334	-	-	-
Total ^{239}Pu fission	2.021	2.172	2.472	2.625	-	-	-
Natural depleted	1.82	1.93	2.23	2.38	-	-	-
Run A							
Subcadmium ^{63}Cu	1.701	1.819	2.130	2.232	-	-	-
Cadmium ratio	17.66	18.65	21.11	21.99	-	-	-
Subcadmium ^{186}W	1.701	1.828	2.123	2.233	-	-	4.307
Cadmium ratio	4.60	4.80	4.93	5.06	-	-	6.74
Subcadmium ^{115}In	1.839	1.989	2.241	2.366	-	-	4.394
Cadmium ratio	2.22	2.34	2.43	2.51	-	-	3.34
Subcadmium ^{55}Mn[a]	1.800	1.917	2.243	2.362	-	-	4.414
Cadmium ratio	16.32	17.13	19.00	19.63	-	-	32.70
Subcadmium ^{176}Lu[a]	2.103	2.208	2.516	2.608	-	-	4.443
Cadmium ratio	103	93	99	102	-	-	165

	Moderator Foils, cm from housing				
	1	3	5	7	9
Subcadmium ^{55}Mn	3.440	3.987	4.266	4.441	4.488
Cadmium ratio	26.28	-	32.84	-	34.54
Subcadmium ^{176}Lu	3.549	3.984	4.312	4.399	4.503
Cadmium ratio	147	-	168	-	165

(a) Thermal column reference foil was lost; activations are normalized to HAMMER computations of Lu/Mn ratio at cell boundary.

TABLE VIII

Foil Activations for 19-Rod Clusters of Type B Fuel with HB-40 Coolant (99.48 mol % D_2O Moderator)

	Fuel Rod Position (see Figure 2)						
	1	2	3	4	5	6	Edge of Cell
Run B							
Total ^{238}U capture	1.771	1.907	2.400	2.448	-	-	-
	1.753	1.900	2.392	2.451	-	-	-
	1.798	1.986	2.474	2.624	-	-	-
	1.779	1.944	2.436	2.552	-	-	-
Subcadmium ^{63}Cu	1.249	1.419	1.820	1.923	-	-	-
Total ^{235}U fission	1.258	1.426	1.809	1.890	-	-	-
Total ^{239}Pu fission	1.410	1.559	2.004	2.104	-	-	-
Natural depleted	1.25	1.42	1.83	1.92	-	-	-
Run A							
Subcadmium ^{63}Cu	1.182	1.356	1.654	1.825	-	-	3.749
Cadmium ratio	18.95	21.39	25.41	28.26	-	-	50.80
Subcadmium ^{186}W	1.184	1.346	1.647	1.806	-	-	3.800
Cadmium ratio	4.55	4.88	5.48	5.76	-	-	8.65
Subcadmium ^{115}In	1.260	1.472	1.765	1.938	-	-	3.898
Cadmium ratio	2.26	2.47	2.69	2.86	-	-	4.06
Subcadmium ^{55}Mn	1.181	1.339	1.658	1.784	-	-	3.761
Cadmium ratio	17.13	18.90	22.62	24.00	-	-	43.63
Subcadmium ^{176}Lu	1.478	1.640	1.952	2.089	-	-	3.893
Cadmium ratio	63.61	70.96	77.52	85.37	-	-	129.50

	Moderator Foils, cm from housing				
	1	3	5	7	9
Subcadmium ^{55}Mn	3.047	3.395	3.604	3.705	3.766
Cadmium ratio	35.53	-	42.26	-	44.06
Subcadmium ^{176}Lu	3.205	3.469	3.683	3.836	3.846
Cadmium ratio	111.57	-	117.58	-	119.68

TABLE IX

Foil Activations for 19-Rod Clusters of Type C Fuel with HB-40 Coolant (99.65 mol % D_2O Moderator)

	Fuel Rod Position (see Figure 2)						
	1	2	3	4	5	6	Edge of Cell
Run B							
Total ^{238}U capture	2.063	2.303	2.781	2.973	-	-	-
	2.082	2.315	2.743	2.974	-	-	-
	2.068	2.314	2.761	2.933	-	-	-
	2.106	2.262	2.706	2.938	-	-	-
Subcadmium ^{63}Cu	1.392	1.570	1.909	2.118	-	-	-
Total ^{235}U fission	1.430	1.114	1.995	2.129	-	-	-
Total ^{239}Pu fission	1.605	1.791	2.193	2.338	-	-	-
Natural depleted	1.40	1.62	1.98	2.16	-	-	-
Run A							
Subcadmium ^{63}Cu	1.347	1.531	1.958	2.154	-	-	-
Cadmium ratio	16.29	18.10	22.50	24.55	-	-	-
Subcadmium ^{186}W	1.353	1.543	1.966	2.153	-	-	4.643
Cadmium ratio	4.00	4.29	4.95	5.18	-	-	8.18
Subcadmium ^{115}In	1.481	1.659	2.125	2.286	-	-	4.745
Cadmium ratio	2.12	2.23	2.52	2.61	-	-	3.88
Subcadmium ^{55}Mn	1.387	1.575	2.026	2.221	-	-	4.664
Cadmium ratio	13.88	15.56	19.14	20.80	-	-	40.18
Subcadmium ^{176}Lu	1.771	1.977	2.418	2.595	-	-	4.865
Cadmium ratio	59.21	64.63	75.22	80.78	-	-	134.22

	Moderator Foils, cm from housing				
	1	3	5	7	9
Subcadmium ^{55}Mn	3.832	4.246	4.459	4.619	4.584
Cadmium ratio	31.9	-	37.42	-	38.43
Subcadmium ^{176}Lu	3.884	4.415	4.643	4.725	4.768
Cadmium ratio	102.5	-	123.55	-	126.19

TABLE X

Foil Activations for 19-Rod Clusters of Type C Fuel with D_2O Coolant (99.66 mol % D_2O Coolant and Moderator)

	Fuel Rod Position (see Figure 2)						
	1	2	3	4	5	6	Edge of Cell
Run B							
Total ^{238}U capture	3.431	3.657	4.277	4.611	-	-	-
	3.465	3.676	4.277	4.570	-	-	-
	3.487	3.663	4.310	4.608	-	-	-
	3.438	3.679	4.305	4.549	-	-	-
Subcadmium ^{63}Cu	2.417	2.600	3.056	3.216	-	-	-
Total ^{235}U fission	2.392	2.558	3.056	3.353	-	-	-
Total ^{239}Pu fission	2.667	2.839	3.305	3.475	-	-	-
Natural depleted	2.52	2.71	3.19	3.35	-	-	-
Run A							
Subcadmium ^{63}Cu	2.219	2.413	2.836	3.025	-	-	-
Cadmium ratio	15.07	16.22	18.49	19.39	-	-	-
Subcadmium ^{186}W	2.235	2.446	2.845	3.033	-	-	5.780
Cadmium ratio	4.13	4.29	4.54	4.62	-	-	6.34
Subcadmium ^{115}In	-	2.596	3.058	3.203	-	-	5.858
Cadmium ratio	-	2.10	2.28	2.32	-	-	3.20
Subcadmium ^{55}Mn	2.339	2.458	2.942	3.081	-	-	5.861
Cadmium ratio	13.41	14.56	16.73	17.17	-	-	30.84
Subcadmium ^{176}Lu	2.878	2.966	3.460	3.601	-	-	6.126
Cadmium ratio	58.22	56.43	65.87	65.30	-	-	103.38

	Moderator Foils, cm from housing				
	1	3	5	7	9
Subcadmium ^{55}Mn	4.548	5.391	5.772	6.021	6.096
Cadmium ratio	23.06	-	29.45	-	31.36
Subcadmium ^{176}Lu	4.980	5.734	6.108	6.294	6.393
Cadmium ratio	80.47	-	92.85	-	98.15

TABLE XI

Foil Activations for 19-Rod Clusters of Type C Fuel with Air Coolant (99.66 mol % D_2O Moderator)

	Fuel Rod Position (see Figure 2)						
	1	2	3	4	5	6	Edge of Cell
Run B							
Total ^{238}U capture	-	-	-	-	-	-	-
Subcadmium ^{63}Cu	2.542	2.707	3.107	3.247	-	-	-
Total ^{235}U fission	-	-	-	-	-	-	-
Total ^{239}Pu fission	-	-	-	-	-	-	-
Natural depleted	-	-	-	-	-	-	-
Run A							
Subcadmium ^{63}Cu	2.307	2.535	2.950	3.076	-	-	-
Cadmium ratio	15.64	16.50	18.41	18.87	-	-	-
Subcadmium ^{186}W	2.400	2.561	2.953	3.068	-	-	-
Cadmium ratio	4.22	4.29	4.45	4.45	-	-	5.87
Subcadmium ^{115}In	2.680	2.781	3.218	3.328	-	-	5.987
Cadmium ratio	2.06	2.09	2.24	2.27	-	-	3.07
Subcadmium ^{55}Mn	2.461	2.659	3.018	3.193	-	-	5.818
Cadmium ratio	14.32	15.21	16.66	17.17	-	-	29.15
Subcadmium ^{176}Lu	3.056	3.186	3.535	3.584	-	-	6.040
Cadmium ratio	55.54	59.50	65.05	61.76	-	-	92.44

	Moderator Foils, cm from housing				
	1	3	5	7	9
Subcadmium ^{55}Mn	4.356	5.200	5.623	5.852	5.922
Cadmium ratio	21.14	-	26.92	-	28.85
Subcadmium ^{176}Lu	4.772	5.504	5.857	6.094	6.191
Cadmium ratio	74.28	-	86.77	-	90.91

TABLE XII

Foil Activations for 19-Rod Clusters of Type E Fuel with HB-40 Coolant (99.64 mol % D_2O Moderator)

	Fuel Rod Position (see Figure 2)						
	1	2	3	4	5	6	Edge of Cell
Run B							
Total ^{238}U capture	0.801	0.894	1.078	1.184	-	-	-
	0.790	0.886	1.075	1.186	-	-	-
Total ^{235}U fission	0.647	0.721	0.916	0.966	-	-	-
Total ^{239}Pu fission	0.763	0.825	1.027	1.072	-	-	-
Natural depleted	0.59	0.65	0.88	0.90	-	-	-
Run A							
Subcadmium ^{63}Cu	0.550	0.617	0.780	-	-	-	-
Cadmium ratio	18.95	20.67	25.10	-	-	-	-
Subcadmium ^{186}W	0.558	0.622	0.781	0.865	-	-	1.768
Cadmium ratio	4.69	4.99	5.52	5.93	-	-	8.41
Subcadmium ^{115}In	0.657	0.710	0.875	1.090	-	-	1.918
Cadmium ratio	2.38	2.47	2.73	3.17	-	-	4.19
Subcadmium ^{55}Mn	0.608	0.668	0.842	0.944	-	-	1.896
Cadmium ratio	18.16	19.27	23.36	26.18	-	-	45.28
Subcadmium ^{176}Lu	0.804	0.865	1.033	1.126	-	-	1.986
Cadmium ratio	73.35	74.26	87.51	91.45	-	-	143.23

	Moderator Foils, cm from housing				
	1	3	5	7	9
Subcadmium ^{55}Mn	1.573	1.738	1.842	1.887	1.929
Cadmium ratio	37.38	-	43.98	-	45.54
Subcadmium ^{176}Lu	1.675	1.833	1.925	1.979	2.012
Cadmium ratio	102.47	-	121.72	-	128.17

TABLE XIII

Foil Activations for 19-Rod Clusters of Type E Fuel with D_2O Coolant (99.65 mol % D_2O Coolant and Moderator)

	Fuel Rod Position (see Figure 2)						
	1	2	3	4	5	6	Edge of Cell
Run B							
Total ^{238}U capture	1.390	1.513	1.719	1.878	-	-	-
	1.443	1.520	1.744	1.896	-	-	-
Total ^{235}U fission	-	1.217	1.217	1.485	-	-	-
Total ^{239}Pu fission	-	1.505	1.657	1.799	-	-	-
Natural depleted	1.04	1.08	1.29	1.38	-	-	-
Run A							
Subcadmium ^{63}Cu	1.017	1.094	1.263	1.358	-	-	-
Cadmium ratio	18.15	19.09	21.17	22.57	-	-	-
Subcadmium ^{186}W	1.028	1.107	1.277	1.375	-	-	2.514
Cadmium ratio	4.96	5.09	5.32	5.47	-	-	6.96
Subcadmium ^{115}In	1.153	1.225	1.356	1.453	-	-	2.543
Cadmium ratio	2.31	2.38	2.48	2.57	-	-	3.46
Subcadmium ^{55}Mn	1.040	1.104	1.293	1.392	-	-	2.477
Cadmium ratio	16.69	17.14	19.59	20.81	-	-	34.20
Subcadmium ^{176}Lu	1.351	1.402	1.580	1.656	-	-	2.616
Cadmium ratio	69.61	68.44	77.44	77.83	-	-	110.79

	Moderator Foils, cm from housing				
	1	3	5	7	9
Subcadmium ^{55}Mn	1.974	2.274	2.422	2.519	2.540
Cadmium ratio	26.09	-	31.92	-	33.68
Subcadmium ^{176}Lu	2.152	2.435	2.555	2.641	2.695
Cadmium ratio	87.41	-	103.37	-	104.81

TABLE XIV

Foil Activations for 19-Rod Clusters of Type E Fuel with Air Coolant (99.66 mol % D_2O Moderator)

	Fuel Rod Position (see Figure 2)						
	1	2	3	4	5	6	Edge of Cell
Run B							
Total ^{238}U capture	1.543	1.616	1.895	1.958	-	-	-
	1.518	1.599	1.823	1.908	-	-	-
Total ^{235}U fission	1.346	1.431	1.618	1.652	-	-	-
Total ^{239}Pu fission	1.643	1.704	1.884	1.943	-	-	-
Natural depleted	1.17	1.23	1.42	1.48	-	-	-
Run A							
Subcadmium ^{63}Cu	1.125	1.199	1.350	1.399	-	-	-
Cadmium ratio	17.63	18.70	19.98	20.82	-	-	-
Subcadmium ^{186}W	1.125	1.199	1.353	1.408	-	-	2.626
Cadmium ratio	4.84	4.92	5.05	5.09	-	-	6.49
Subcadmium ^{115}In	1.252	1.319	1.463	1.527	-	-	2.723
Cadmium ratio	2.19	2.26	2.35	2.40	-	-	3.26
Subcadmium ^{55}Mn	1.144	1.208	1.390	1.454	-	-	2.608
Cadmium ratio	16.09	16.82	18.63	19.60	-	-	31.78
Subcadmium ^{176}Lu	1.475	1.535	1.694	1.744	-	-	2.735
Cadmium ratio	51.36	65.58	68.51	68.29	-	-	99.63

	Moderator Foils, cm from housing				
	1	3	5	7	9
Subcadmium ^{55}Mn	2.005	2.364	2.537	2.645	2.654
Cadmium ratio	27.15	-	34.20	-	35.63
Subcadmium ^{176}Lu	2.219	2.546	2.676	2.765	2.819
Cadmium ratio	91.40	-	105.50	-	110.68

TABLE XV

Foil Activations for 31-Rod Clusters of Type C Fuel with D_2O Coolant (99.63 mol % D_2O Coolant and Moderator)

	Fuel Rod Position (see Figure 2)						
	1	2	3	4	5	6	Edge of Cell
Run B							
Total ^{238}U capture	2.787	2.940	3.248	3.506	4.192	4.103	-
	2.776	2.886	3.181	3.433	4.080	4.157	-
	2.885	2.999	3.318	3.574	4.174	4.225	-
	2.802	2.956	3.218	3.449	4.075	4.102	-
Subcadmium ^{63}Cu	1.618	1.741	1.958	2.100	2.527	2.537	-
Subcadmium ^{55}Mn	-	-	-	-	-	-	-
Total ^{235}U fission	1.654	1.754	1.973	2.113	2.552	2.558	-
Total ^{239}Pu fission	1.866	2.001	2.260	2.409	2.880	2.828	-
Natural depleted	1.67	1.78	2.04	2.17	2.61	2.68	-
Run A							
Subcadmium ^{63}Cu	1.489	1.617	1.794	1.991	2.361	2.398	-
Cadmium ratio	9.13	9.75	10.63	11.46	13.08	13.28	-
Subcadmium ^{186}W	1.497	1.636	1.787	1.988	2.353	2.374	4.911
Cadmium ratio	2.90	2.97	3.05	3.20	3.35	3.37	4.49
Subcadmium ^{115}In	1.733	1.790	2.033	2.187	3.487	2.607	4.995
Cadmium ratio	1.67	1.67	1.75	1.81	1.86	1.93	2.46
Subcadmium ^{55}Mn	1.520	1.614	1.824	1.970	2.367	2.329	4.829
Cadmium ratio	8.45	8.76	9.64	10.10	11.65	11.57	20.08
Subcadmium ^{176}Lu	2.011	2.113	2.358	2.493	2.905	2.893	5.271
Cadmium ratio	35.55	36.06	38.72	40.56	44.90	45.19	65.66

	Moderator Foils, cm from housing				
	1	3	5	7	9
Subcadmium ^{55}Mn	3.695	4.324	4.761	4.897	4.950
Cadmium ratio	16.17	-	20.19	-	21.42
Subcadmium ^{176}Lu	4.231	4.879	5.180	5.351	5.343
Cadmium ratio	55.55	-	68.51	-	68.84

TABLE XVI

Foil Activations for 31-Rod Clusters of Type C Fuel with HB-40 Coolant (99.61 mol % D_2O Moderator)

	Fuel Rod Position (see Figure 2)						
	1	2	3	4	5	6	Edge of Cell
Run B							
Total ^{238}U capture	1.622	1.700	1.940	2.090	2.642	2.694	-
	1.503	1.708	1.921	2.048	2.562	2.617	-
	1.640	1.752	1.976	2.161	2.720	2.708	-
	1.597	1.724	1.958	2.117	2.698	2.717	-
Subcadmium ^{63}Cu	0.890	0.999	1.209	1.327	1.792	1.784	-
Total ^{235}U fission	0.856	1.046	1.253	1.329	1.854	1.797	-
Total ^{239}Pu fission	1.086	1.205	1.413	1.534	2.009	1.976	-
Natural depleted	0.90	1.00	1.23	1.34	1.79	1.81	-
Run A							
Subcadmium ^{63}Cu	0.843	0.941	1.147	1.269	1.692	1.701	-
Cadmium ratio	10.35	11.24	13.20	14.42	18.31	18.37	-
Subcadmium ^{186}W	0.853	0.660	1.171	1.287	1.700	1.719	3.759
Cadmium ratio	2.85	3.05	3.38	3.52	4.03	4.08	6.09
Subcadmium ^{115}In	0.985	0.607	1.301	1.430	1.858	1.889	3.922
Cadmium ratio	1.72	1.78	1.89	1.97	2.19	2.21	3.12
Subcadmium ^{55}Mn	0.851	0.956	1.169	1.276	1.725	1.740	4.151
Cadmium ratio	8.98	10.11	11.67	12.62	16.25	16.28	33.37
Subcadmium ^{176}Lu	1.157	1.294	1.516	1.638	2.075	2.089	5.612
Cadmium ratio	38.19	42.05	47.29	50.13	58.10	57.75	138.59

	Moderator Foils, cm from housing				
	1	3	5	7	9
Subcadmium ^{55}Mn	3.217	3.574	3.766	3.877	3.909
Cadmium ratio	26.08	-	29.39	-	30.49
Subcadmium ^{176}Lu	3.478	3.777	3.973	4.059	4.081
Cadmium ratio	88.71	-	96.64	-	100.47

TABLE XVII

Foil Activations for 31-Rod Clusters of Type E Fuel with D_2O Coolant (99.63 mol % D_2O Coolant and Moderator)

	Fuel Rod Position (see Figure 2)						
	1	2	3	4	5	6	Edge of Cell
Run B							
Total ^{238}U capture	1.043	1.112	1.198	1.314	1.526	1.536	-
	1.065	1.111	1.216	1.312	1.517	1.545	-
Total ^{235}U fission	.7815	.8326	.9092	1.0006	1.1594	1.1733	-
Total ^{239}Pu fission	.9754	1.0377	1.1087	1.2084	1.2553	1.3812	-
Natural depleted	0.69	0.73	0.82	0.87	1.03	1.05	-
Run A							
Subcadmium ^{63}Cu	0.667	0.705	0.789	0.856	1.010	1.024	-
Cadmium ratio	11.33	11.68	12.79	13.74	15.46	15.78	-
Subcadmium ^{186}W	0.677	0.709	0.800	0.868	1.022	1.030	2.027
Cadmium ratio	3.49	3.51	3.68	3.79	3.93	3.98	4.96
Subcadmium ^{115}In	0.791	0.819	0.928	1.019	1.141	1.126	2.119
Cadmium ratio	1.83	1.84	1.93	2.01	2.08	2.07	2.69
Subcadmium ^{55}Mn	0.694	0.713	0.808	0.876	1.035	1.037	2.010
Cadmium ratio	10.60	10.60	11.67	12.49	13.96	14.10	22.88
Subcadmium ^{176}Lu	0.928	0.965	1.069	1.102	1.265	1.273	2.149
Cadmium ratio	47.41	47.14	50.90	51.93	56.77	56.52	75.98

	Moderator Foils, cm from housing				
	1	3	5	7	9
Subcadmium ^{55}Mn	1.536	1.791	1.911	1.999	2.023
Cadmium ratio	18.40	-	22.72	-	24.23
Subcadmium ^{176}Lu	1.740	1.930	2.066	2.120	2.136
Cadmium ratio	62.12	-	77.07	-	82.75

TABLE XVIII

Foil Activations for 31-Rod Clusters of Type E Fuel with HB-40 Coolant (99.59 mol % D_2O Moderator)

	Fuel Rod Position (see Figure 2)						
	1	2	3	4	5	6	Edge of Cell
Run B							
Total ^{238}U capture	0.533	0.579	0.650	0.695	0.891	0.862	-
	0.541	0.579	0.663	0.714	0.903	0.877	-
Total ^{235}U fission	0.407	0.448	0.502	0.555	0.712	0.737	-
Total ^{239}Pu fission	0.516	0.554	0.624	0.681	0.847	0.871	-
Natural depleted	0.33	0.36	0.47	0.50	0.65	0.64	-
Run A							
Subcadmium ^{63}Cu	0.338	0.372	0.440	0.483	0.639	0.626	-
Cadmium ratio	13.40	14.36	16.43	17.98	22.19	21.83	-
Subcadmium ^{186}W	0.353	0.388	0.456	0.496	0.652	0.640	1.419
Cadmium ratio	3.66	3.81	4.17	4.31	4.91	4.76	6.84
Subcadmium ^{115}In	0.392	0.436	0.525	0.538	0.735	0.705	1.460
Cadmium ratio	1.90	2.00	2.15	2.18	2.52	2.46	3.42
Subcadmium ^{55}Mn	0.346	0.376	0.454	0.493	0.670	0.640	1.401
Cadmium ratio	11.87	12.38	14.24	15.70	19.72	18.77	33.13
Subcadmium ^{176}Lu	0.483	0.524	0.604	0.651	0.804	0.788	1.479
Cadmium ratio	46.69	50.37	55.27	57.84	72.19	64.96	103.13

	Moderator Foils, cm from housing				
	1	3	5	7	9
Subcadmium ^{55}Mn	1.152	1.274	1.344	1.370	1.385
Cadmium ratio	27.93	-	33.34	-	33.31
Subcadmium ^{176}Lu	1.235	1.336	1.418	1.439	1.447
Cadmium ratio	76.83	-	99.44	-	89.80

COMPUTATION OF LATTICE PARAMETERS

All lattice computations reported here were performed with the SRL HAMMER code[7]. This code provides one-dimensional integral transport calculations. Lattice cell computations are based on 54 fast energy groups, (>0.62 ev) and 30 thermal energy groups (<0.62 ev) and are "first-principle" calculations in the sense that they are made directly from the cell geometry and the microscopic cross sections of the cell materials. Effective resonance neutron cross sections are calculated by the Nordheim ZUT and TUZ codes[11]. Up to 20 spatial regions are allowed. Reaction rates for the 84 total energy groups are collapsed into four (or fewer) energy groups for overall lattice calculations. Group cross sections, migration areas, and bucklings are obtained from the solution of the few-group critical equation via the FLOG code, the HAMMER version of the FOG code[12].

LATTICE COMPUTATIONS - CYLINDRICAL MODEL

Because the HAMMER system is currently restricted to a single spatial dimension, it was necessary to construct suitable one-dimensional models of the rod clusters used in the experiments. Models composed of concentric cylindrical rings were used since they were expected to be more accurate than the time-honored method of homogenizing into a single large rod. The model was also chosen to approximate the essential physics characteristics of the rod, i.e. to distribute the fuel spatially so as to give closely the proper thermal neutron distributions, and to position the fuel surfaces so as to give approximately the correct resonance capture. However, since the exact thermal and resonance effects cannot be mocked up simultaneously, the model chosen was a compromise.

A pictorial presentation of the model is given in Figure 10, which shows its application to the 31-rod cluster. Hexagonal micro-cells are constructed by lines joining the rod centers, and fuel material is separated from coolant, clad, and void. Starting from the center of this model, the fuel and the coolant clad and void are then placed in alternating rings constructed in such a fashion as to conserve areas and average atom densities. The area of the complete cluster (Regions 1-8 in Figure 10) is simply the sum of the microcells.

Alternative ring models have also been used. One, employed at Combustion Engineering[13] (CE), homogenizes all coolant, clad, and void material contained inside the housing tube and positions each fuel ring such that its radial midpoint is at the average radius of the rod centers comprising that ring. Average atom densities are

also conserved in this model. Figure 11 shows a typical example of the effect of the model on the microscopic thermal neutron distribution in a cell. The combined effect of differences in fuel placement and coolant homogenization is shown separately and in combination. The effect of the model on resonance capture is illustrated in Table XIX. The computed values of ρ shown are the ratio of epicadmium to subcadmium neutron capture in ^{238}U.

TABLE XIX

Computed ρ Values for Different Fuel Cluster Models
19-Rod Clusters, 9.33-inch Δ Lattice Pitch, Fuel Type E, HB-40 Coolant

Model		Calculated
Fuel	Coolant	ρ
SRL	SRL	0.3386
SRL	CE	0.3467
CE	SRL	0.3432
CE	CE	0.3482
SRL Corrected		0.362

For the last entry in this table a hand computation was made to correct for known deficiencies in the cluster surface-to-mass ratio in the SRL model. The corrections assume the validity of the effective surface-to-mass (S/M ratio) concept and utilize earlier SRL numerical techniques for evaluation of this parameter for the actual fuel cluster. These numerical techniques define the exterior surface as that which a "rubber band" would conform to if stretched around the assembly and allowed to contract until it touches fuel. The interior surface is defined as the total rod surface minus the exterior surface. The effectiveness factor is that evaluated by numerical methods for an infinite array of the individual rods at the same pitch (0.597-inch). Similar computations were performed for the SRL cylindrical model. For each case the corresponding resonance integrals for ^{238}U were obtained from the standard expression,

$$RI = A + B\sqrt{S/M}$$

using Hellstrand's values[14] of A and B. The calculated values of ρ_{28} were then multiplied by the ratio RI_{Rods}/RI_{Ring}. The corrections to ρ_{28} ranged from 3% to 7% for the 19-rod cluster and were less than 1% for the 31-rod cluster.

The effect on material buckling of the computed ρ_{28} corrections was also evaluated. Changes in ρ_{28} were converted first to changes of resonance escape probability, and thence to k_∞, and finally to B^2. Computed HAMMER values provided the basis for the computed corrections.

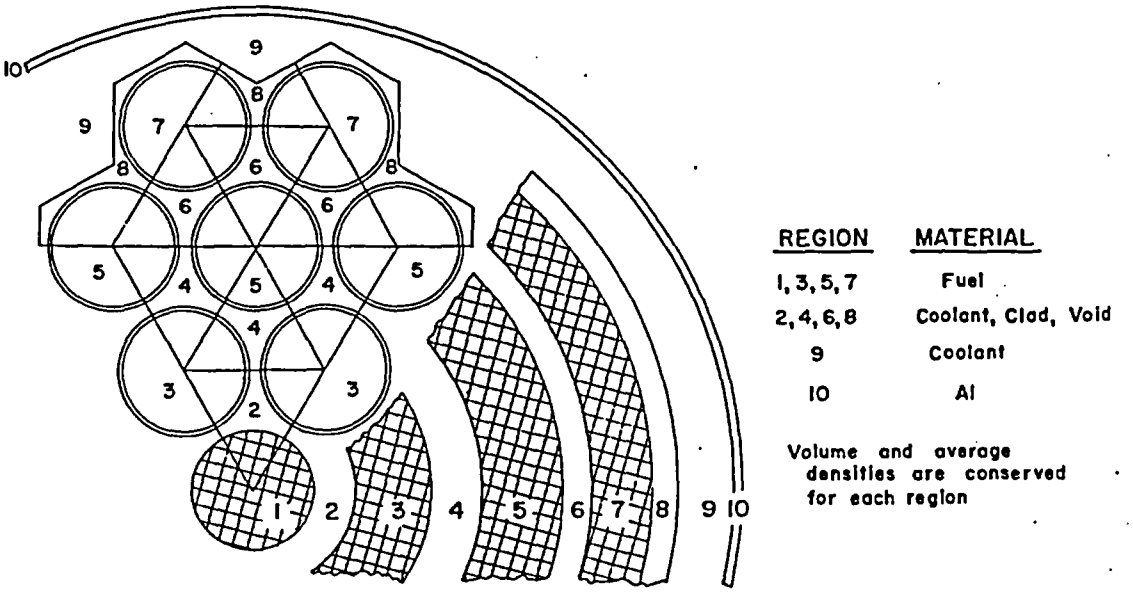

FIG. 10 SRL CONCENTRIC RING MODEL FOR HAMMER COMPUTATIONS (31-Rod Cluster)

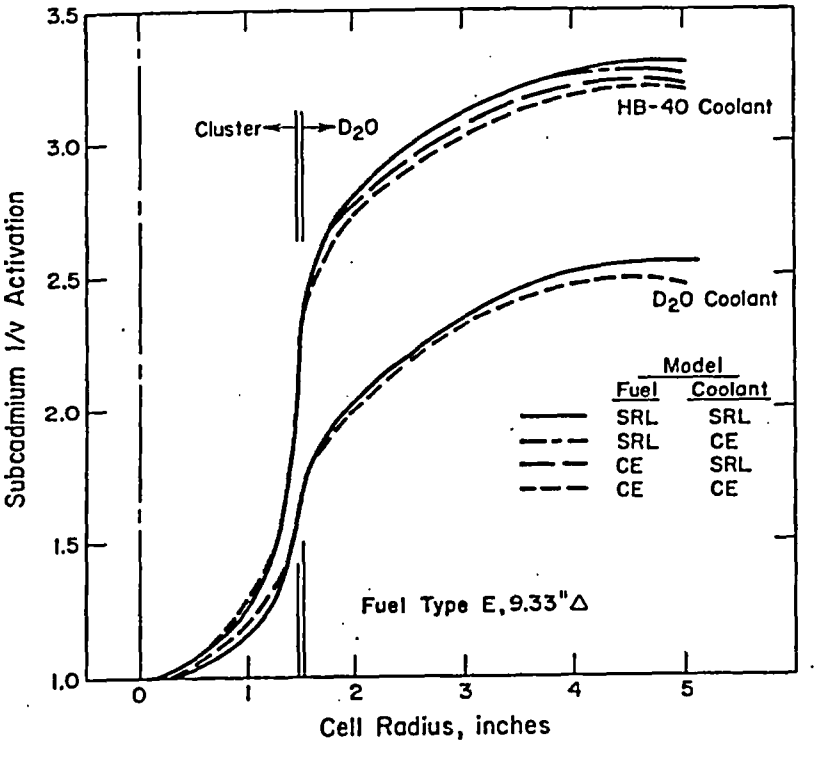

FIG. 11 HAMMER COMPUTATION OF INTRACELL FLUX PROFILE SHOWING SENSITIVITY TO RING MODEL USED

The ring model dimensions are detailed in Table XX for both the 19- and 31-rod clusters. The average atom densities for the coolant-clad mixture are also given. A bulk moderator temperature of 20°C and a purity of 99.75 mol % D_2O were assumed. Fuel densities and isotopic concentrations were those of Table I.

The HAMMER calculations for the test lattices are listed in Table XXI. The values in the table are those computed for the basic SRL ring model except for the buckling values, which also include a listing (inside parentheses) for the effective surface correction just outlined. Parameters have the normal meaning except for the slowing down area, τ, which includes epithermal neutron absorption in the removal cross section and resonance escape, and ρ, which includes all epithermal capture rather than ^{238}U alone.

The sensitivities of the bucklings to variations from the assumed plutonium concentrations in the test fuel were also determined by the HAMMER computations. The computations were based on a 5% reduction in the absolute plutonium content of each fuel type. The sensitivities are tabulated for representative cases.

TABLE XX

SRL Ring Models of 19- and 31-Rod Clusters

Region	19-Rod Cluster		31-Rod Cluster	
	OD, inches	Material	OD, inches	Material
1	0.5	UO_2	0.5	UO_2
2	0.824	CC[a]	0.824	CC
3	1.4761	UO_2	1.4761	UO_2
4	1.8617	CC	1.8617	CC
5	2.5428	UO_2	2.5423	UO_2
6	2.7326	CC	2.7844	CC
7	3.02	Coolant	3.2792	UO_2
8	3.08	Al	3.4904	CC
9	-	D_2O	3.892	Coolant
10	-	-	4.000	Al
11	-	-	-	D_2O

(a) CC = Coolant-clad mixture as shown below in atoms/barn centimeter, 20°C, (Applicable to both cluster sizes)

Isotope	D_2O-H_2O	HB-40	Air
H	0.0001091	0.03645	-
D	0.04357	-	-
O	0.02184	-	-
C	-	0.02983	-
Al	0.01796	0.01796	0.01796

TABLE XXI

HAMMER Calculations of Test Lattices

Fuel Type	Coolant	Thermal Parameters: η	f	Σ_a, cm^{-1}	D, cm	L^2, cm^2	Epithermal Parameters: Σ_a, cm^{-1}	$\nu\Sigma_f$, cm^{-1}	Σ_R, cm^{-1}	D, cm	τ, cm^2	p	Lattice Parameters: k_∞	B^2, m^{-2}(a)	ϕ_{epi}/ϕ_{th}	$\Delta B^2/\Delta Pu$, $m^{-2}/\%Pu$
							19-Rod Cluster, 9.33-inch Triangular Lattice Pitch									
A	D_2O	1.2891	.9614	.004136	.8381	202.6	.001753	.000925	.009711	1.2846	112.1	.8471	1.1301	4.238(4.03)	.4622	.072
A	HB-40	1.2893	.8670	.003757	.7517	200.1	.001902	.001008	.011744	1.2599	92.3	.8606	1.0358	1.283(1.01)	.3283	
A	Void	1.2888	.9623	.004232	.8621	203.7	.001586	.000889	.009209	1.3793	127.8	.8531	1.1398	4.306(4.17)	.5005	
B	D_2O	1.3092	.9610	.004100	.8386	204.5	.001646	.000920	.009755	1.2858	112.8	.8556	1.1566	5.029(4.84)	.4631	.082
B	HB-40	1.3095	.8656	.003732	.7517	201.4	.001785	.001002	.011795	1.2611	92.9	.8686	1.0580	2.055(1.80)	.3295	
B	Void	1.3089	.9618	.004194	.8627	205.7	.001488	.000884	.009245	1.3807	128.7	.8614	1.1662	5.041(4.90)	.4478	
C	D_2O	1.3856	.9640	.004362	.8391	192.4	.001684	.000970	.009618	1.2860	113.8	.8510	1.2222	7.286(7.06)	.5167	.086
C	HB-40	1.3859	.8752	.003916	.7539	192.5	.001824	.001052	.011644	1.2615	93.7	.8646	1.1264	4.542(4.25)	.3658	
C	Void	1.3852	.9649	.004475	.8628	192.8	.001523	.000932	.009112	1.3812	129.9	.8568	1.2323	7.191(7.02)	.4997	
D	D_2O	1.1427	.9534	.003558	.8370	235.2	.001564	.000857	.010075	1.2838	110.3	.8657	1.0166	.506(.37)	.3573	
D	HB-40	1.1418	.8426	.003342	.7456	223.1	.001701	.000940	.012124	1.2587	91.0	.8770	.91217	-3.014(-3.18)	.2571	
D	Void	1.1424	.9541	.003618	.8623	238.4	.001409	.000824	.009546	1.3779	125.8	.8714	1.0249	.720(.63)	.3455	
E	D_2O	1.3212	.9597	.003971	.8416	211.9	.001610	.000955	.009796	1.2850	112.7	.8588	1.1723	5.401(5.22)	.4517	
E	HB-40	1.3204	.8614	.003632	.7522	207.1	-	-	-	-	92.8	.8714	1.0673	2.341(2.10)	.3220	
E	Void	1.3210	.9605	.004056	.8664	213.6	.001453	.000917	.009269	1.3798	128.7	.8645	1.1819	5.385(5.25)	.4364	
							31-Rod Cluster, 9.33 Triangular Lattice Pitch									
A	D_2O	1.2937	.9625	.006180	.8479	137.2	.002520	.001180	.008837	1.2756	112.3	.7781	1.0726	3.038(3.07)	.7291	.082
A	HB-40	1.2936	.8529	.005599	.7084	126.5	.002705	.001326	.011860	1.2412	85.2	.8143	.9894	-.533(-.50)	.4683	
A	Void	1.2911	.9624	.005416	.8790	162.3	.002029	.001087	.008389	1.4056	134.9	.8052	1.1043	3.637(3.58)	.6101	
B	D_2O	1.3138	.9621	.006133	.8489	138.4	.002357	.001175	.008867	1.2775	113.8	.7900	1.1028	4.225(4.25)	.7304	
B	HB-40	1.3137	.8513	.005567	.7082	127.2	.002533	.001316	.011986	1.2426	85.6	.8255	1.0141	.7011(.73)	.4689	
B	Void	1.3133	.9642	.006367	.8917	140.0	.002107	.001129	.008144	1.4128	137.8	.7945	1.1155	4.290(4.23)	.8286	
C	D_2O	1.3895	.9651	.006506	.8489	130.5	.002412	.001248	.008749	1.2775	114.5	.7839	1.1626	6.777(6.81)	.8099	.096
C	HB-40	1.3897	.8614	.005821	.7110	122.2	.002586	.001389	.0011793	1.2431	86.5	.8202	1.0779	3.900(3.93)	.5173	
C	Void	1.3889	.9672	.006778	.8911	131.5	.002158	.001199	.007998	1.4132	139.2	.7875	1.1753	6.589(6.53)	.9212	
D	D_2O	1.1400	.9542	.004994	.8467	160.0	.002238	.001081	.009284	1.2748	110.6	.8058	.9705	-1.169(-1.14)	.5596	
D	HB-40	1.1398	.8266	.004994	.7000	140.2	.002413	.001226	.012419	1.2392	83.5	.8373	.8725	-6.274(-6.25)	.3668	
D	Void	1.1396	.9563	.005452	.8922	163.7	.001992	.001039	.008511	1.4090	134.1	.8103	.9822	-.641(-.58)	.6337	
E	D_2O	1.3185	.9603	.005863	.8519	145.3	.002303	.001229	.008950	1.2763	113.4	.7953	1.1158	4.638(4.67)	.6995	
E	HB-40	1.3182	.8455	.005381	.7079	131.6	.002473	.001369	.012025	1.2416	85.6	.8294	1.0187	.9167(.95)	.4527	
E	Void	1.3180	.9624	.006072	.8964	147.6	.002056	.001180	.008189	1.4116	137.8	.7993	1.1285	4.648(4.59)	.7924	
							31-Rod Cluster, 12.12-inch Triangular Lattice Pitch									
A	D_2O	1.2876	.9518	.003351	.8349	249.2	.001812	.001028	.09591	1.2814	112.4	.8411	1.1206	3.468(3.50)	.3798	.082
A	HB-40	1.2886	.8381	.002899	.7576	261.0	.002067	.001159	.011818	1.2556	90.4	.8512	1.0026	.07992(.11)	.2454	
A	Void	1.2599	.9813	.003658	.8541	233.5	.001593	.000890	.008984	1.4062	133.0	.8494	1.1339	3.746(3.69)	.4429	
B	D_2O	1.3077	.9513	.003327	.8356	251.1	.001712	.001024	.009591	1.2830	113.5	.8486	1.1458	4.134(4.16)	.3820	.092
B	HB-40	1.3088	.8367	.002885	.7564	262.2	.001948	.001149	.011931	1.2567	90.5	.8596	1.0240	.7254(.75)	.2465	
B	Void	1.2790	.9812	.003628	.8547	235.6	.001500	.000884	.009019	1.4079	133.9	.8574	1.1597	4.404(4.34)	.4439	
C	D_2O	1.3841	.9547	.003501	.8355	238.7	.001749	.001073	.009514	1.2829	113.9	.8447	1.2111	6.103(6.13)	.4217	.102
C	HB-40	1.3852	.8465	.002992	.7582	253.4	.001989	.001202	.011798	1.2569	91.2	.8558	1.0904	2.757(2.79)	.2714	
C	Void			.003843	.8540	222.2	.001534	.000931	.008902	1.4083	135.0	.8530	1.2258	6.348(6.29)	.2493	
D	D_2O	1.1420	.9431	.002954	.8340	282.3	.001633	.000958	.009926	1.2807	110.8	.8588	1.0078	.2119(.24)	.2998	
D	HB-40	1.1412	.8132	.002648	.7508	283.5	.001862	.001085	.012202	1.2544	89.2	.8676	.8829	-3.441(-3.41)	.1958	
D	Void	1.1416	.9447	.003022	.8573	283.7	.001444	.000930	.009298	1.3914	129.6	.8656	1.0200	.5145(.45)	.3297	
E	D_2O	1.3207	.9499	.003239	.8379	258.7	.001680	.001058	.009655	1.2819	113.1	.8518	1.1616	4.490(4.52)	.3744	
E	HB-40	1.3199	.8323	.002823	.7564	267.9	.001909	.001187	.011951	1.2558	90.6	.8622	1.0327	.972(1.00)	.2424	
E	Void	1.3202	.9523	.003341	.8598	257.3	.001504	.001035	.009043	1.3908	131.9	.8574	1.1755	4.638(4.58)	.4134	

(a) B^2(corrected) - numbers in parentheses

COMPARISON OF EXPERIMENT TO THEORY

PDP Bucklings

A graphical display of the experimental bucklings (abscissa) and the magnitude by which each measurement differs from the HAMMER calculated value (ordinate) is shown in Figure 12. No systematic variation is observed with respect to either fuel or coolant composition. For the 31-rod clusters at a triangular lattice pitch of 12.12 inches, the agreement on average between experiment and the calculations is good. At the closer pitch of 9.33 inches, however, the measured values for 31-rod clusters are about 0.5 m^{-2} higher than the predicted values and the 19-rod clusters give values about 0.2 m^{-2} higher than predicted.

SE Temperature Coefficients

Computed buckling values for the SE temperature coefficient studies with 19-rod clusters of Type B fuel are displayed with the experimental bucklings in Figure 5. These lattices coincide with the PDP lattices of 19-rod clusters of D_2O-cooled Type B fuel except for the omission of the cluster housing tubes in the SE measurements. The HAMMER computed values are based on the SRL ring model with the previously discussed correction for resonance capture. The slopes of the computed curves fit the measured data within experimental error. The computed absolute bucklings, however, disagree with the measurements at the 9.33-inch pitch and in the same direction as for the PDP measurements. The close agreement between buckling measurements in the two facilities is indicated by the identical difference, 0.38 m^{-2}, between measured and calculated bucklings for this lattice.

Activation Experiments

Experimental and HAMMER calculated intracell activation profiles are plotted in Figures 13 and 14. The experimental activations are the subcadmium manganese activations listed in Tables VI through XVII as corrected for perturbations caused by the introduction of foil packets and the presence of end caps in the Pu-bearing rods, and for self-shielding in the foils located in the bulk moderator.

The flux corrections for the fuel rods were determined by a computational model in which the end caps, foils, and voids at each foil packet location were homogenized into a single plane foil with an isotropic source at both surfaces. The thermal flux depression calculated for this composite foil was then compared to that calculated for a uranium oxide or plutonium-uranium oxide foil of the same thickness. The latter case corresponds to the desired flux depression

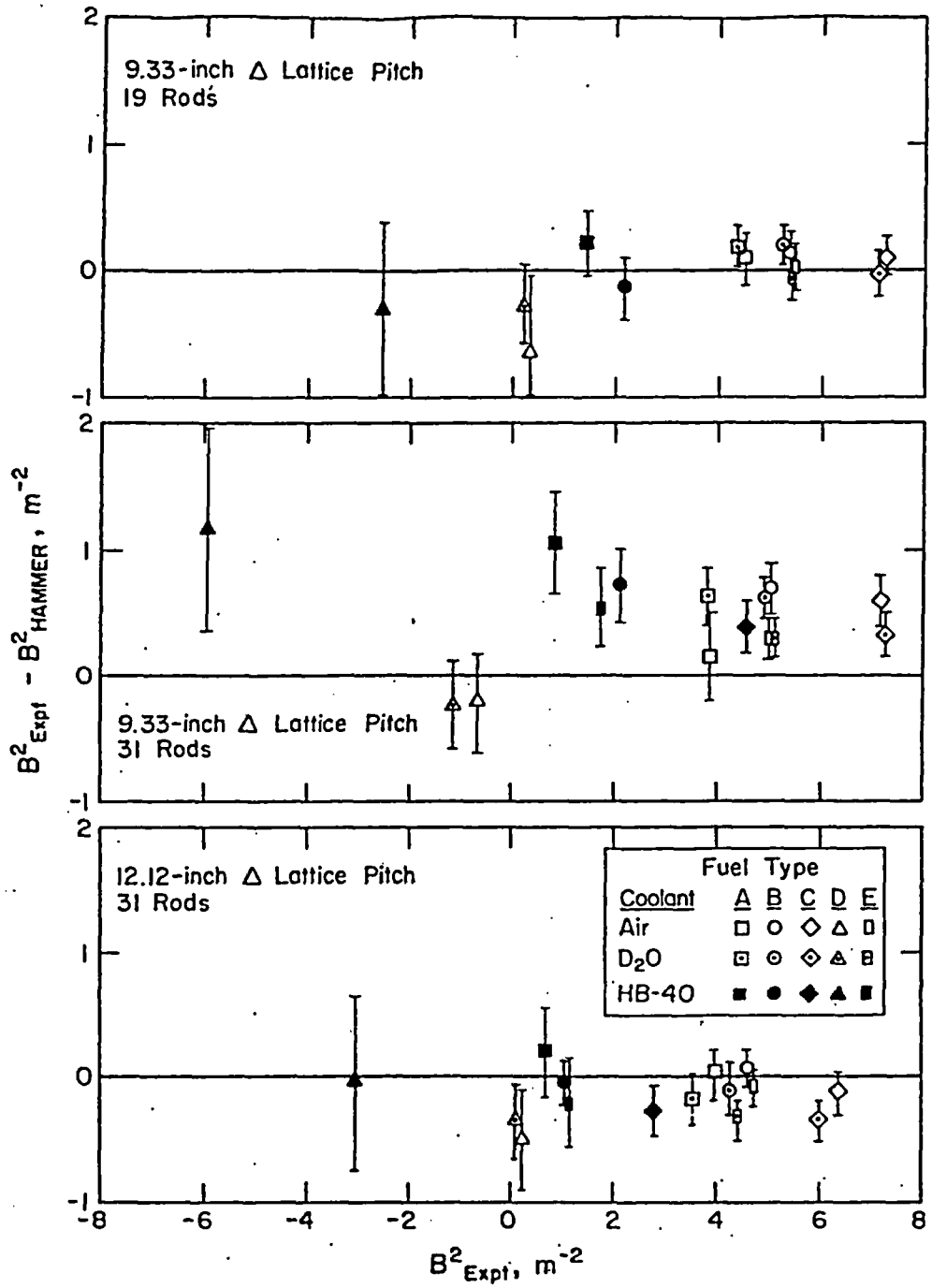

FIG. 12 COMPARISON OF COMPUTED TO MEASURED BUCKLINGS
All bucklings given for 99.75 mol % D_2O

- 51 -

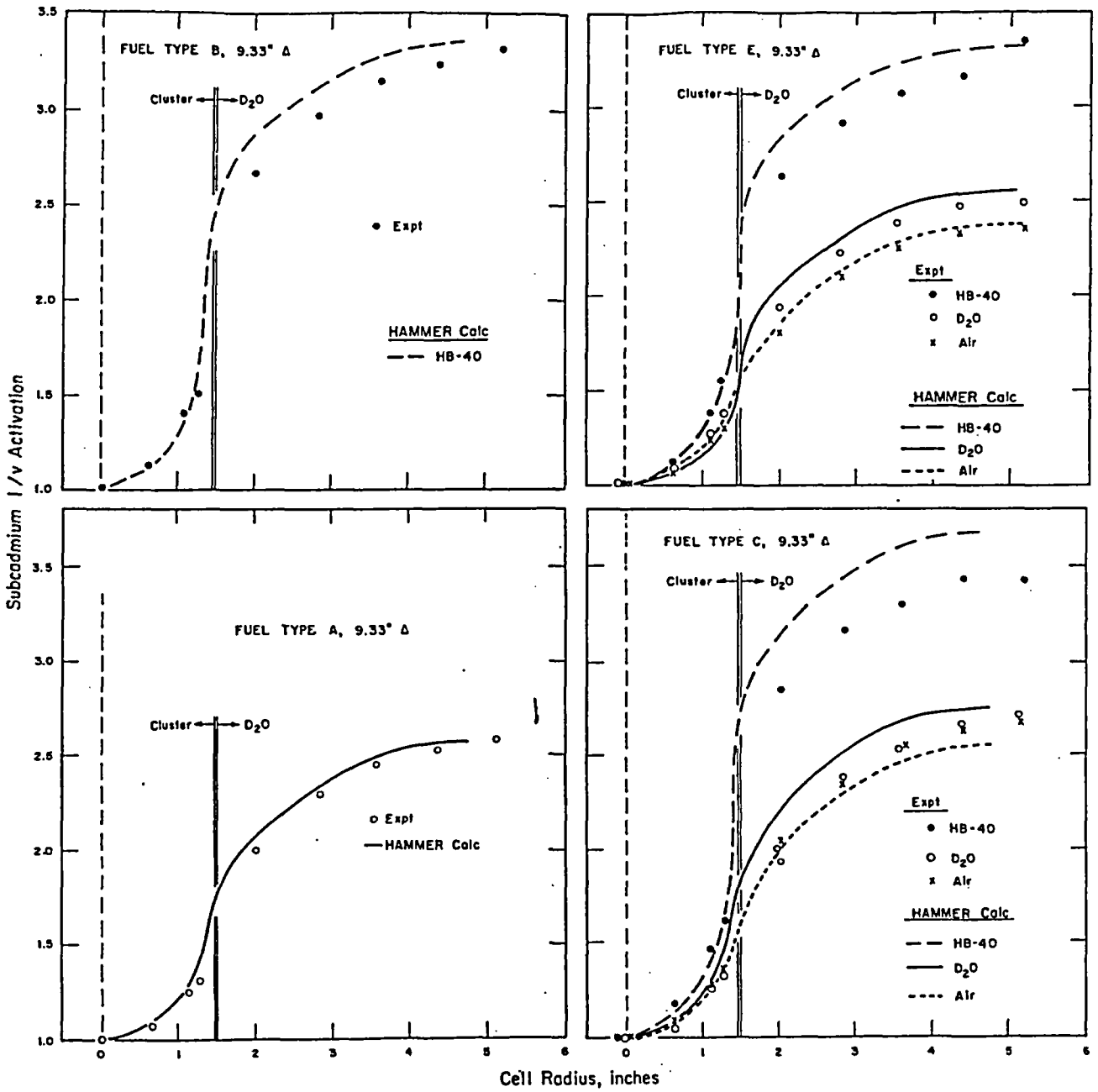

FIG. 13 THERMAL NEUTRON ACTIVATION PROFILES FOR 19-ROD CLUSTERS

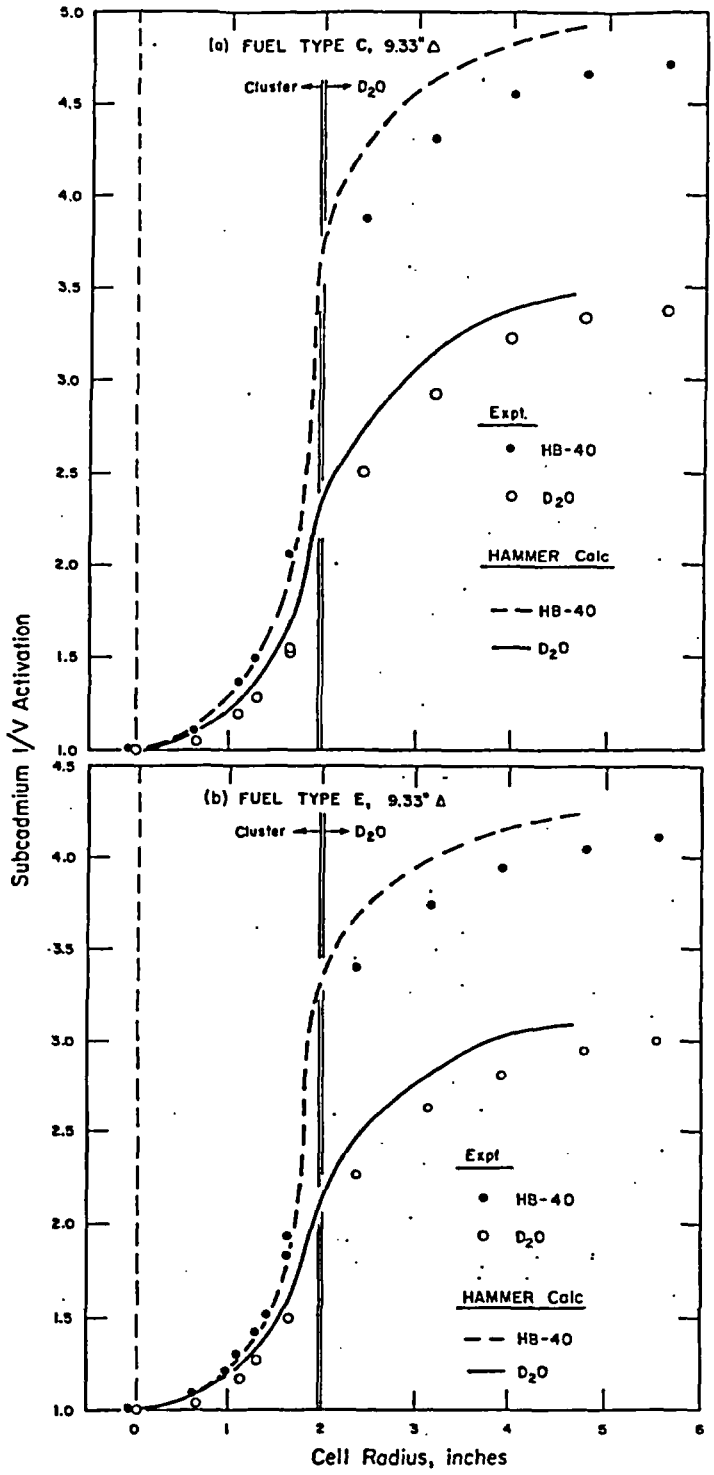

FIG. 14 THERMAL NEUTRON ACTIVATION PROFILES FOR 31-ROD CLUSTERS

in a uniform uninterrupted rod. The results indicated that the flux in a copper foil was depressed approximately 2.0% in relation to the flux in the uniform rod for Type E fuel, but was 0.4% higher in a copper foil than in uniform fuel rods of Types A, B, and C fuel. For a manganese foil the flux was 1.5% higher in the foil than in a uniform rod of Type E fuel and 2.4% higher in the foil than in a uniform rod of Types A, B, or C fuel.

The HAMMER computed activation profiles are based on the SRL geometric ring model discussed earlier. The scattering kernels used were the Nelkin Kernel for deuterium in D_2O[15] and the Ardente-Nelkin Benzene Kernel[16] for hydrogen in HB-40. Both kernels have been found to give good agreement with SRL measurements of diffusion coefficients[17,18]. The average radial position for the fuel in the computational model differs slightly from that of the rods in the cluster. In Figures 13 and 14, the data points plotted are fuel rod averages at the midpoint radius of each rod. The computed curves within the cluster are for fuel only (the fuel-to-coolant fine structure and the hyperfine structure within both are omitted). The computed curves are also distorted so that computed fuel ring averages coincide with the radial position of the rods. The computed curve is drawn as a smooth curve through the indicated points. The curve thus represents a pointwise comparison to the measured data points rather than a true flux profile through the cluster. Experiment and computations are normalized at the central fuel rod.

The agreement between measured and computed activations within the fuel clusters is quite good for all lattices studied, indicating that HAMMER, with the SRL ring model, is adequate for the prediction of the flux and fission power distribution within the cluster. Also the agreement between the calculated and experimental activations throughout the cell is quite good for the D_2O and gas-cooled lattices. There is, however, a systematic discrepancy for the organic-cooled lattices, with the computations consistently overestimating the magnitude of the flux peaking in the bulk moderator. Computations with somewhat altered ring models suggest that part of this effect is due to the model. The CE ring model discussed earlier has the advantage for thermal flux profiles of giving the proper average radius for each hexagonal ring of fuel. Flux profile computations comparing the two models were shown in Figure 11. The best physical model for activation profiles is believed to be the CE geometry with the SRL treatment of coolant and cladding. This combination differs at most by 2% from the SRL model for the example in Figure 11. The direction is to give better agreement with the measurements. The difference is approximately 1% for D_2O coolant and negligible for gas coolant (not shown).

Thermal Neutron Temperature Index

The comparison of HAMMER predicted spectral indices to the measured spectral indices for the Lu-Mn combinations was straightforward. Subcadmium activities for both detector materials were directly comparable to the computed activities. Analogous comparisons for the ^{239}Pu-^{235}U combinations were, however, less straightforward. First, because of the limitation of plutonium foil material, no cadmium-covered foils were included in the experiments. Thus, it was necessary to rely on HAMMER computations for the epicadmium correction. Further, since HAMMER gives only fuel average values of epicadmium capture, it was also necessary to assume that the epicadmium distribution was independent of position for both fissionable isotopes. A second complication which affects both the basic interpretation of the measurements and the cadmium ratio corrections is the dependence of the isotopic distribution of fission products on the fissioning neutron energy. It has been tacitly assumed that over the energy range of these measurements the fission product distribution changes are negligible; i.e. that a measurement of relative fission product activities of ^{239}Pu and ^{235}U (considered separately) is a measurement of relative fission rates. This assumption is known not to be fully valid for either isotope with respect to epicadmium and subcadmium neutrons. There is also some doubt of its validity within the subcadmium region where different distributions may prevail between the thermal 1/v component and the first (subcadmium) resonance for each isotope. Further work remains to determine this difference, but it is expected to be significantly smaller than for the higher energy resonances.

The spectral index comparisons for the combination Lu-Mn foils are shown in Figures 15 and 16. Indices derived for the ^{239}Pu-^{235}U foils are shown in Figures 17 and 18. The HAMMER computations properly predict the qualitative behavior of spectral hardening but consistently overestimate the magnitude of the effect. The discrepancy appears to be independent of the type of fuel or coolant, thus indicating that the difficulties probably arise from the cluster geometry rather than from any special problems with plutonium or organic coolant.

The hardest spectrum, as indicated by the maximum value of the index, is always that in the central fuel rod of the cluster and higher values are generally observed for organic than for D_2O or air. This latter effect of the organic coolant is at first sight surprising inasmuch as the organic is a better moderator with greater thermalizing power (energy exchange per collision) than either D_2O or air. The explanation lies in the diffusion properties of the different coolants. The diffusion length for the cluster, treated as a whole, is given by the expression

$$L \propto \sqrt{\frac{D}{\Sigma_a}}$$

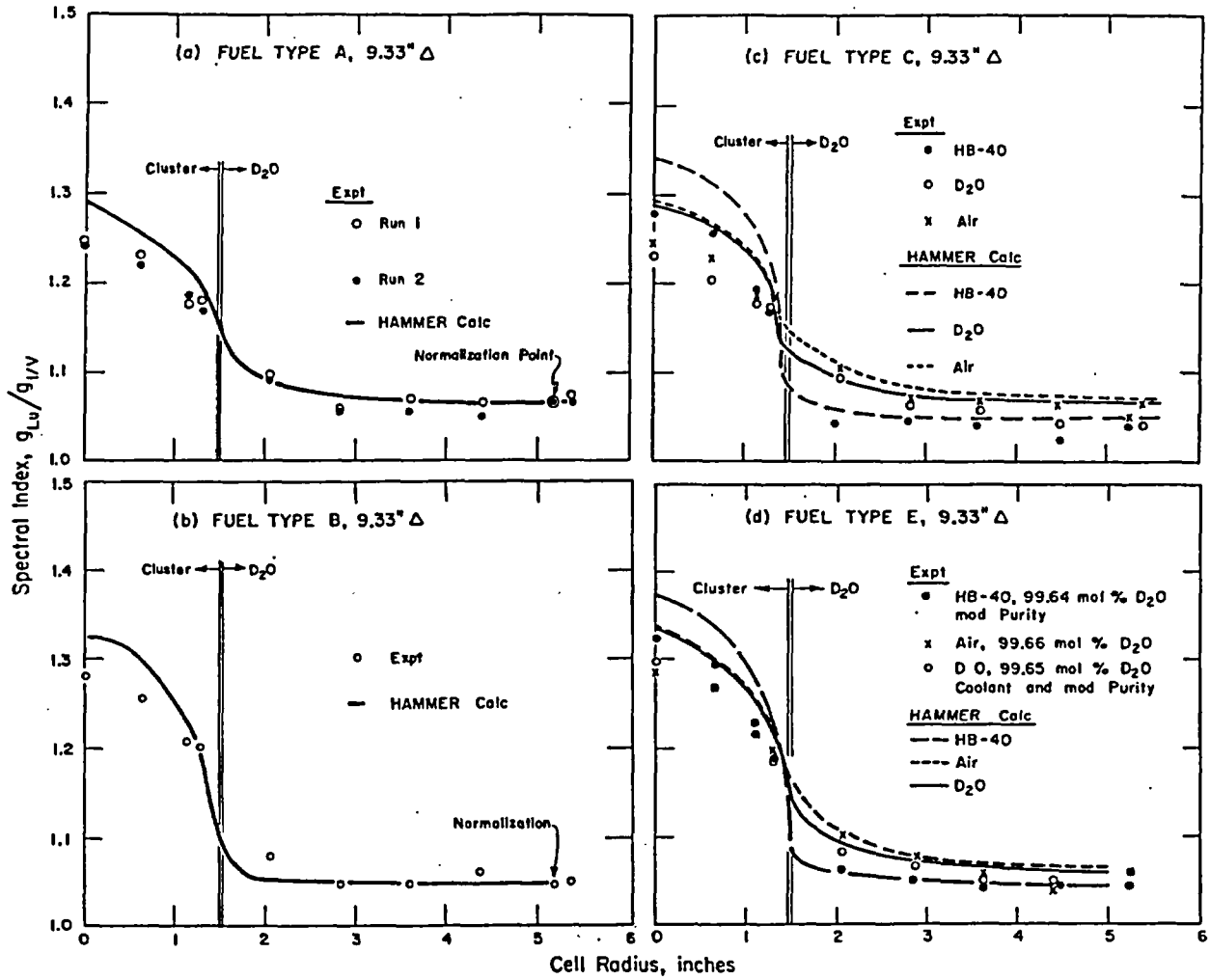

FIG. 15 Lu-Mn NEUTRON TEMPERATURE INDEX PROFILES FOR 19-ROD CLUSTERS

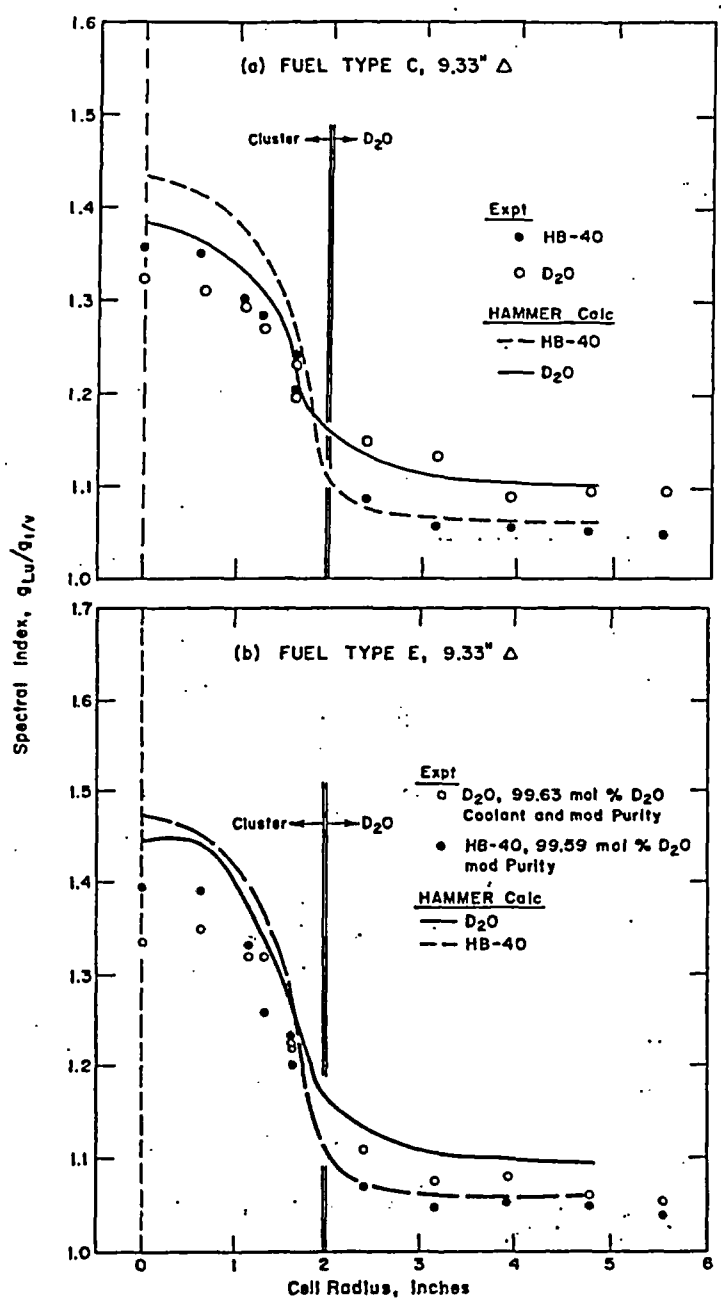

FIG. 16 Lu-Mn NEUTRON TEMPERATURE INDEX PROFILES FOR 31-ROD CLUSTERS

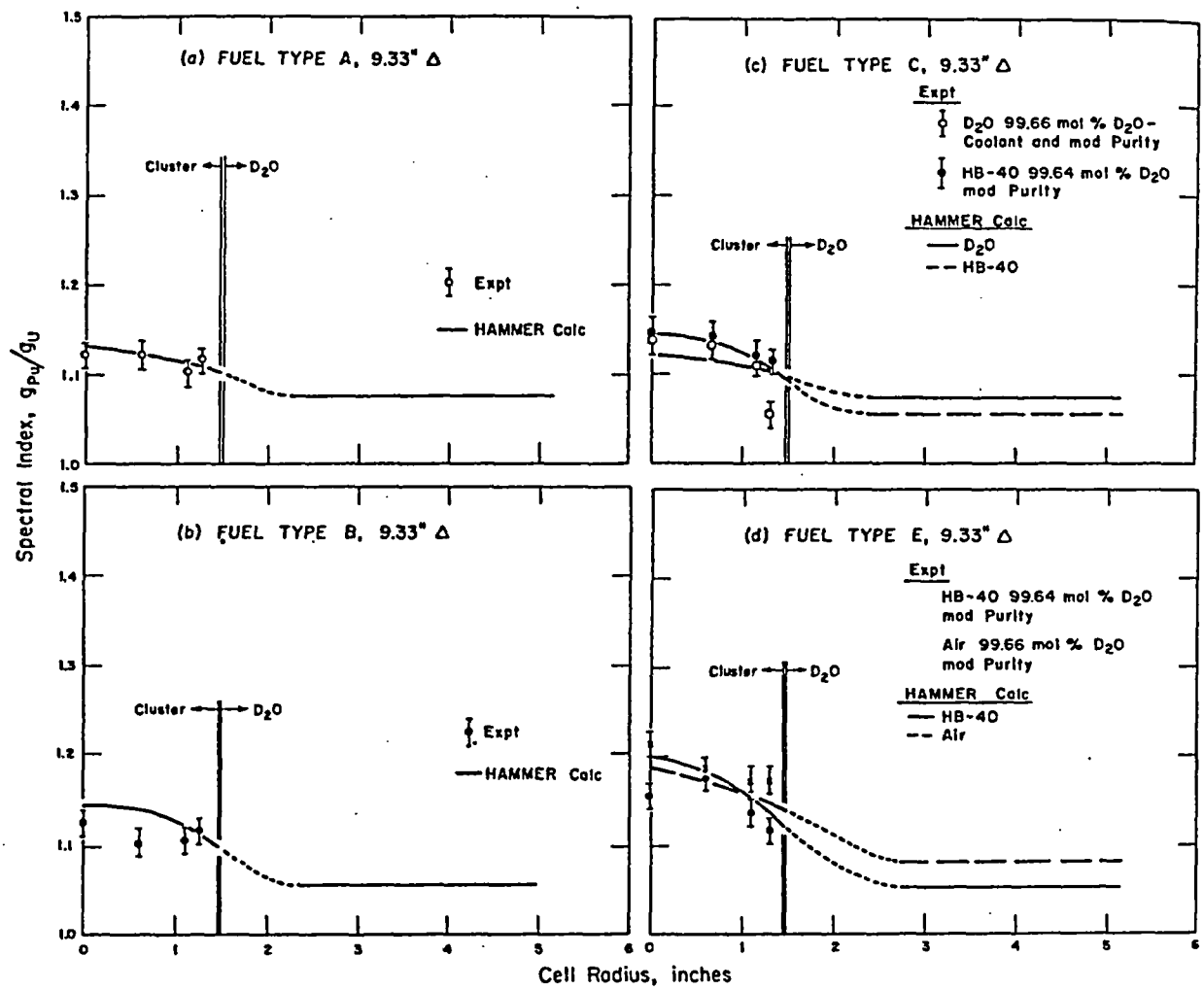

FIG. 17 ^{239}Pu-^{235}U NEUTRON TEMPERATURE INDEX PROFILES FOR 19-ROD CLUSTERS

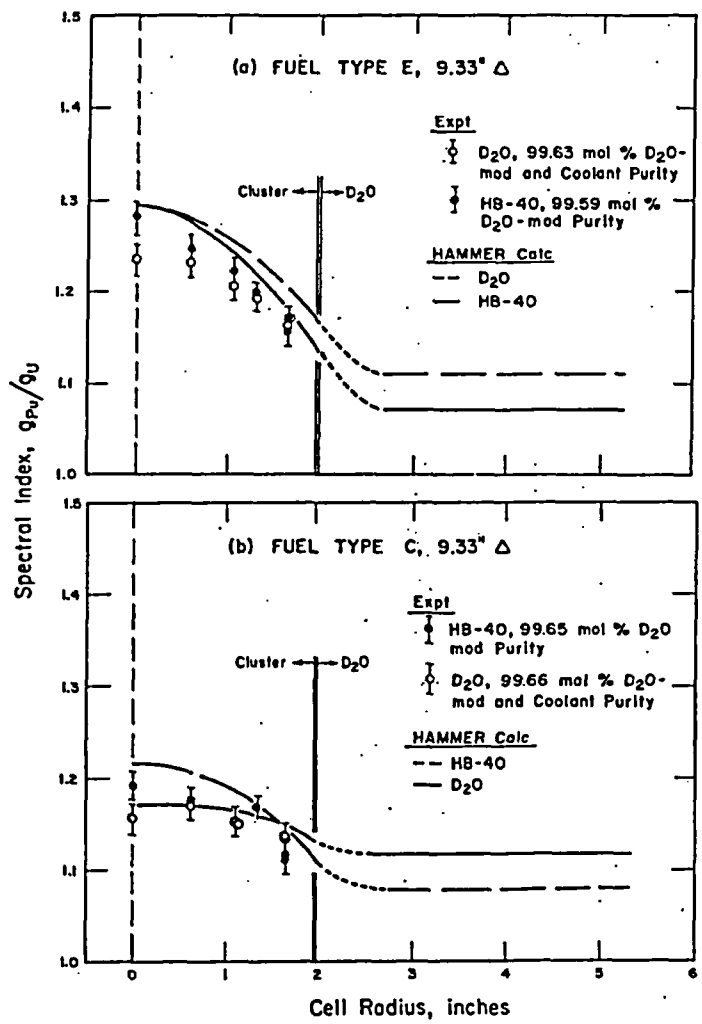

FIG. 18 ^{239}Pu-^{235}U NEUTRON TEMPERATURE INDEX PROFILES FOR 31-ROD CLUSTERS

This equation can be considered to apply for each neutron energy. With all three coolants the macroscopic absorption cross section, Σ_a, varies approximately as 1/v where v is the neutron speed. The diffusion coefficient D is independent of energy for the gas-cooled cases, varies slowly with energy for D_2O ($D \propto v^{0.3}$) and very strongly for organic ($D \propto v^{1.0}$). The diffusion length thus is most strongly energy dependent for the organic-cooled case, being shortest for very slow neutrons. The effect, then, in organic is for the intensity of the slow neutrons (short diffusion length) incident on the cluster to fall off more rapidly with penetration into the cluster than does the intensity of the faster (long diffusion length) neutrons. The effect of the hydrogen in the organic is thus to act as a filter on the incident Maxwellian distribution, admitting the higher energy neutrons into the cluster and scattering the lower energy ones back into the bulk moderator. It should be noted, however, that in agreement with the higher moderating power of the organic coolant the cell-averaged neutron temperature is lower for organic coolants than for gas or D_2O. The lower temperature in the bulk moderator more than compensates for the hardening within the cluster.

The Westcott spectral model and integral cross sections[19] are frequently used[20] for conversion of foil activations ratios. However, in the case of the Pu-bearing fuels, self-shielding effects by the low lying, (~0.3 ev) resonance in ^{239}Pu severely distort the thermal neutron energy spectrum from that of the Westcott model, and hence make it difficult to obtain meaningful neutron temperatures. An example of such distortion is illustrated in Figure 19 where the HAMMER calculated spectrum in the central rod of a Pu-bearing fuel cluster is compared to two versions of the Westcott spectrum model. The neutron temperature in the Westcott model was adjusted to fit the HAMMER values near the peak of the Maxwellian distribution. The r-value was chosen to coincide with the flux at the highest speed interval in the THERMOS subprogram of HAMMER. The ^{239}Pu self-shielding is seen to cause a significant deviation over the normalized speed range from 2 to 5 units, with a maximum error of a factor of 3 at the ^{239}Pu resonance.

Fast Fission Effect

In order to make direct comparisons between measurements and computations, only the ratios between ^{235}U and ^{238}U fissions were considered in the fast fission evaluations. Both measurements and computations were normalized to the fission ratios prevailing in the ^{238}U and ^{235}U isotopes in nonperturbing natural uranium foils. This quantity is indicated as δ_0 in Table V. In order to indicate the overall effect on the lattice, the computed normal value of δ defined as the ratio of ^{238}U fissions to ^{235}U plus Pu fissions is also given in Table VI. The measured and computed ratios are in general agreement for the 19-rod clusters, but the computations overestimate the number of fast fissions for the 31-rod clusters.

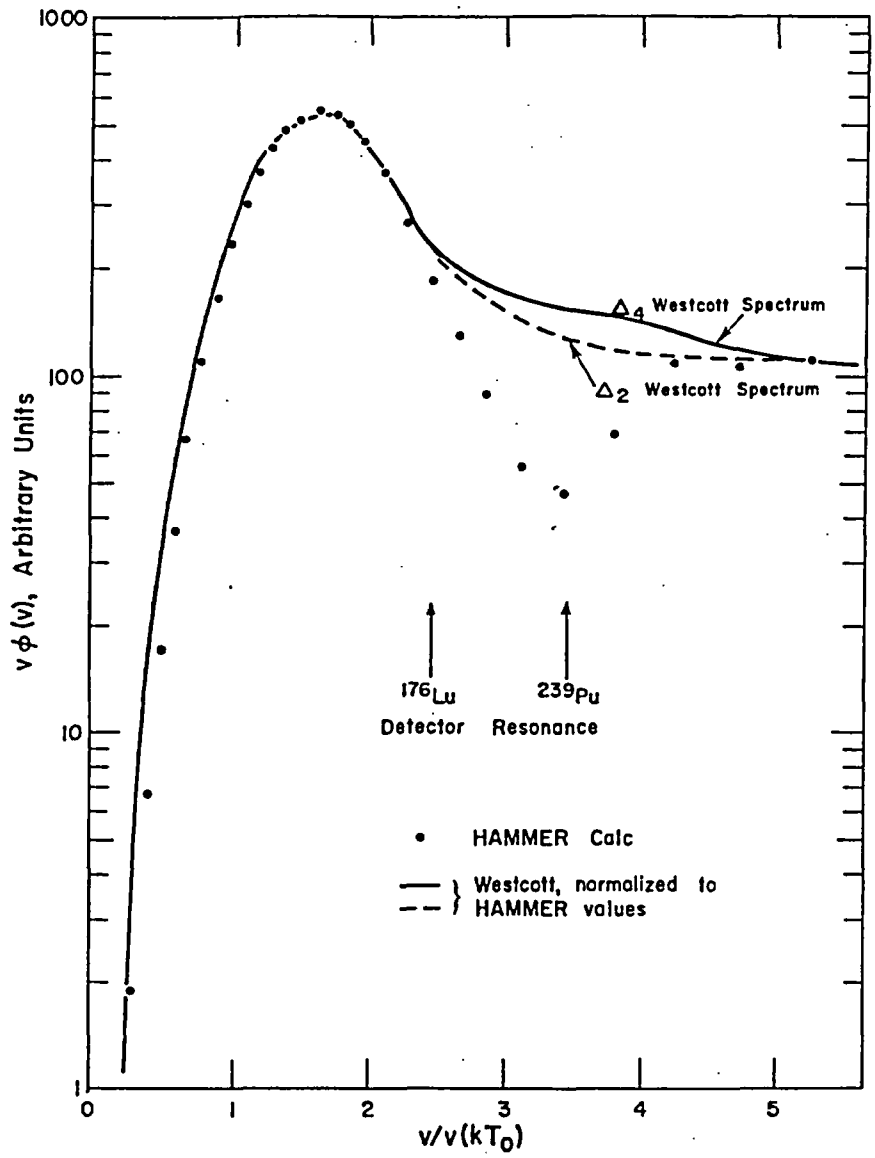

FIG. 19 COMPARISON OF HAMMER SPECTRUM TO WESTCOTT MODEL [19]
(Center Rod, Type C Fuel, 31-Rod Cluster, HB-40 Coolant)

Resonance Capture

Measured and calculated values of ρ, the ratio of epicadmium-to-subcadmium ^{238}U capture are given in Table VI. The values of ρ from the "corrected" HAMMER results are, on the average, approximately 5% lower than the measured values with no systematic variations being evident with fuel type, cluster size, or coolant (only one lattice pitch, 9.33 inches triangular, was used). This discrepancy is in the same direction and consistent with the magnitude of the discrepancy in the buckling comparison.

Table V also lists ^{238}U captures normalized to ^{235}U fissions. The comparison to computed values is made by the quantity C*

$$C^* \equiv \frac{[Ng\sigma_a]^{238}}{[Ng\sigma_f]^{235}} \times \frac{\text{238 Activity in fuel}}{\text{235 Fission activity in fuel}}$$

$$\times \frac{\text{235 Fission activity in reference}}{\text{238 Activity in reference}}$$

where the activities are fuel average and thermal column reference activities, and "g" is the Westcott "g" factor. The atom number densities refer to the fuel rods and the effective cross sections to the thermal reference flux. Fission product activities were obtained directly from ^{235}U-Al alloy foils and by subtracting the depleted uranium foil activities from the paired natural uranium foil activities in both locations. The paired foils have the advantage that the foils are the same foils used to determine ^{238}U capture and thus the physical location is identical. The disadvantage is that counting statistics were generally poorer for this method.

The agreement between the experiments and the computations is seen to be fairly good except for the ^{235}U-Al measurements on the Type E fuel, where a loading error is suspected. Since C* is dominated by thermal rather than resonance effects, it is not inconsistent that there should be reasonable agreement here and lack of agreement in ρ.

The coincident discrepancy in resonance capture and buckling suggests that the method of computing resonance capture is in error. The overall method and the cross sections, however, appear to be verified by the good agreement observed for D_2O-moderated rods of natural uranium metal[21] and/or tubes of natural uranium oxide[22]. This fact suggests that the discrepancy may be due largely to a failure of the cluster model. Computations explicitly for cluster geometries would be invaluable for determining the basis of the disagreement.

APPENDIX A
CHEMICAL AND ISOTOPIC ANALYSES

Determination of the plutonium content of the various fuel types posed special problems. In addition to values obtained by material balance of plutonium and uranium used in the fuel preparation, chemical assays were made of samples taken from the process line and the finished product. Such assays were made by Oak Ridge National Laboratory (ORNL), Nuclear Fuel Services (NFS), and the Savannah River Laboratory (SRL). Values obtained by ORNL and NFS are included in Table XXI, but since these disagreed with the more extensive studies made at Savannah River they are not included with the values summarized in Table I.

The relative abundance of the various plutonium isotopes was obtained by straightforward mass spectrometric methods. The results obtained by the Analytical Chemistry Division of SRL are shown in Table XXII. Three separate techniques were employed[23] to determine plutonium content. The primary method employed at SRL is the use of a scanning coulometer. In the coulometric analysis, plutonium ions in solution are quantitatively reduced from the 4+ state to the 3+ state by the addition of electrons. The scanning feature permits the separation of the effect for plutonium, which is essentially instantaneous, from slower, time-dependent reductions of impurity

TABLE XXII

Comparison of Different Chemical Assays of Type A Fuel

Laboratory	Material	Wt % U	Wt % Pu	Pu/U Weight Fraction
SRL	Powder	87.45	.255	.00292
	Blend 1	87.37	.258	.00293
	Avg	87.41	.256	.00293
NFS	Blend 1			.00241
				.00252
				.00259
				.00271
	Avg			.00255
ORNL	Blend 1			.00336
SRL	Powder	87.20	.258	.00296
	Blend 2	87.28	.258	.00296
	Avg	87.24	.258	.00296
NFS	Blend 2			.00283
				.00286
				.00279
				.00269
	Avg			.00279
ORNL	Blend 2			.00335
SRL	Pellet 3163-1-2	87.96	.258	.00294
ORNL				.00304
ORNL				.00311
	Avg			.00307

ions such as iron. Nonetheless, the presence of rather large iron impurities (Table II) is believed to cause the major uncertainty in these measurements and in the nonscanning coulometric method employed by NFS.

The two alternate methods used by the SRL Analytical Chemistry Division were intended primarily as a check of the scanning coulometer and were not used for all samples. The first of these consisted of an assay by counting of alpha particles in these samples. Multichannel pulse height distributions were obtained to correct for alpha-emitting impurities (believed to be ^{241}Am). The final method of plutonium assay consisted of adding a known number of ^{242}Pu atoms to a sample and determining the plutonium isotopic distribution in a mass spectrometer. The results of all methods of analyses are summarized in Table XXIII. The three SRL methods are seen to give consistent results.

TABLE XXIII

Summary of Plutonium Analyses for Fuel Types A, B, and C

Fuel Type	Sample Designation	Plutonium Content, mg Pu/g total oxide: Material Balance	Coulometric Analyses	Gross Alpha Counting Analyses[a]	Isotopic Dilution	Isotopic Analysis: Pu Isotope	Wt %
A	Composite I	2.76	2.60				
	Composite II		2.58				
	3163-3-03		2.62				
	A-21884		2.57	2.59			
	A-21885		2.58	2.57			
	A-3163-1-1		2.58	2.62			
			(Mean value = 2.59 ±0.02)[b]			238	<0.02
						239	77.77
						240	19.37
						241	2.53
						242	0.311
B	Composite I	2.39	2.28	2.29	2.27		
	Composite II		2.28	2.29	-		
	Composite III		2.29	2.29	2.28		
	Master Mix						
	No. 3, Blend 1		2.32			238	~0.01
	No. 3, Blend 9		2.32			239	93.01
	3163-3					240	6.15
	Blend 16		2.28			241	0.791
	3163-3					242	0.044
	Blend 20		2.29				
	3163-3						
	Blend 28		2.28				
			(Mean value = 2.29 ±0.01)[b]			238	0.01
						239	93.01
						240	6.16
						241	0.791
						242	0.042
C	Composite I	3.32	2.98	2.96			
	Composite II		2.98	2.96			
	Composite III		2.98	2.96			
	36543		2.84				
	36548		3.02				
	36515		2.80				
	36525		2.89				
			(Mean value = 2.93 ±0.07)[b]			238	0.02
						239	93.14
						240	6.11
						241	0.697
						242	0.033

(a) Mounts for gross alpha counting were examined on a pulse height analyzer. Data indicated that ~6% of activity was ^{241}Am (and/or ^{238}Pu). This was subtracted from gross alpha activity and the remainder considered as arising from plutonium of masses 239 and 240.

(b) Standard deviation by range method at 95% confidence limit.

APPENDIX B
UNIFORMITY OF PLUTONIUM DISTRIBUTION

Although macroscopic uniformity of Pu distribution had been assured by coprecipitation of the PuO_2-UO_2, considered to be microscopic agglomeration of Pu atoms was possible. The major nuclear effect of such agglomeration would be increased resonance self-shielding by the ^{240}Pu atoms. Thus, the effect would be most pronounced for the Type A fuel.

A simple model was used to estimate the self-shielding effect. In this model, all of the plutonium was assumed to be in the form of uniformly sized spheres of PuO_2 randomly distributed in a UO_2 matrix. The calculations indicated that with this model, Pu agglomeration would introduce perceptible errors in the measured parameters, notably buckling, only if the spheres had radii in excess of 0.002 cm. For Type A fuel, a 0.002-cm sphere would, an average, have associated with it approximately 120 μg of UO_2. The experimental test for agglomeration thus consisted of breaking up sample pellets of the Type A oxide to determine the Pu content per unit weight of the individual fragments.

Initial attempts to weigh the fragments failed, and it was necessary to devise activation methods to determine weights. For this determination, three sets of foils were irradiated in a uniform thermal neutron flux: 1) the Pu-bearing samples, 2) comparably sized but unweighed samples of natural and depleted uranium, and 3) large weighed foils of the natural and depleted uranium. All small foils were counted at an integral bias of 500 kev on the day following the irradiation. This count, being due solely to ^{235}U and ^{239}Pu fission products, served to establish the relative assay of these two isotopes. Three days following the irradiation, the small foils were again counted, this time with a window of 90-116 kev and at a separate simultaneous integral bias of 500 kev. The window count, after being corrected for fission product activity, served as an assay of the relative ^{238}U content and thus the relative weight of the individual particles. The fission product correction in the window was made under the assumption that the energy distribution of ^{239}Pu fission products is similar to that for ^{235}U. The >500 kev count thus served as a monitor of total fission product activity. The relative weight of the small natural and depleted foils was determined by the integral bias count and the known depletion ratio, and, after correcting both count rates for background, the two foil activities were corrected to a uniform weight. The factor relating the integral count to that part of the window count due to fission products was determined by simply taking the ratio of the difference counts of the two foils. The corrected window counts then gave relative weights of all small foils, including the natural-depleted uranium pair. The ^{235}U component of the fission product count of

the Pu-bearing foils, which must be subtracted to give the Pu assay, was determined from the fission product activity of the natural-depleted pair, the relative foil weights, and the known ^{235}U depletion ratio of the Type A fuel. The only further information required was the absolute determination of the foil weights which up to this point had been determined only on a relative basis. The absolute value was established by counting of the 2.3-day ^{239}Np activity for the large weighed natural and depleted foils several weeks after the irradiation on the same counter and under the same conditions as for the small fragments. The known half-life was used to correct the activity back to the activity at the time the small foils had been counted.

A total of 29 of the Pu-bearing foils were assayed. These foils varied in weight between 203 and 592 μg, with a mean weight of 321 μg. The Pu content per unit weight of these foils varied from 24% below to 49% above the mean value, with an overall standard deviation from the mean of 13.1%. The specific Pu distribution is shown graphically in Figure 20. This figure also shows computed Poisson statistical distributions based on the previously discussed models of randomly distributed uniform spheres of PuO_2. (The discrete distributions are shown as smooth curves to simplify the comparison.) The distribution is seen to agree closely with the computation for 64 spheres per particle. This also compares well with the 58 spheres per particle derived from the measured standard deviation and an assumed normal statistical distribution. The latter number gives an equivalent radius of 7.7×10^{-4} cm, well below the 2×10^{-3} cm limit required. No appreciable error due to agglomeration is thus anticipated.

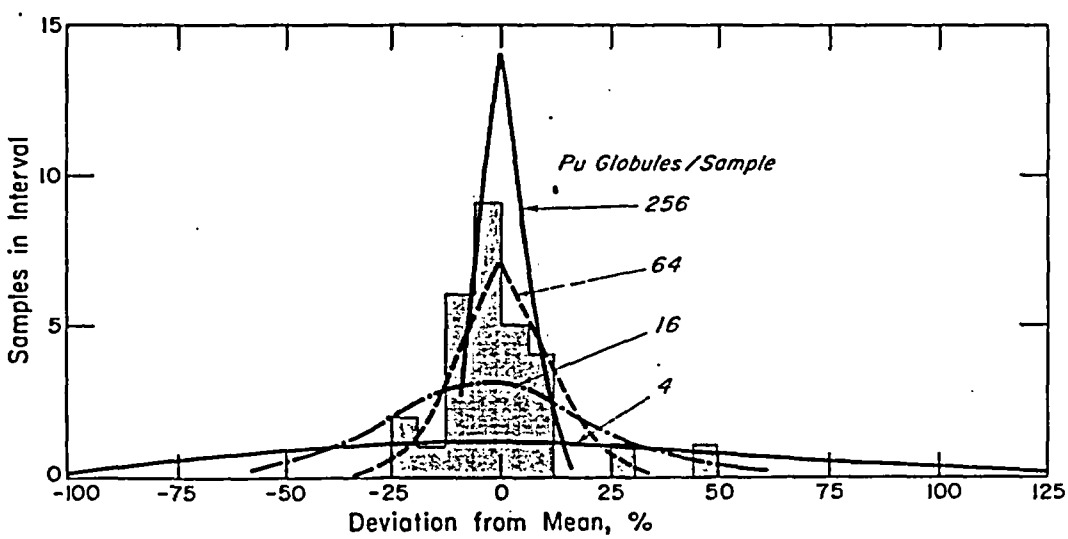

FIG. 20 ASSAY OF PLUTONIUM AGGLOMERATION IN TYPE A FUEL

APPENDIX C
SUBSTITUTION BUCKLING MEASUREMENTS

The three methods used to analyze the substitution buckling measurements performed in the PDP were discussed in the Lattice Measurement Section of this report. This appendix details the methods used to treat the analytical results and to assign probable error limits.

For each fuel type, cluster size, and lattice pitch, several critical runs were made differing in the number of test assemblies or their geometrical arrangement. The arrangements were tailored primarily to analysis by the method of Persson, and often included measurements to which the two-group and HERESY methods were not readily applicable. Thus the confidence placed in any one method must reflect the number of cases analyzed and the number of test fuel assemblies used.

For each test lattice (combination of fuel type, cluster size, and lattice pitch) and each method of analysis, a probable error limit was assigned. The probable error limits necessarily reflect some judgment on the part of the experimenters and are based on the sample size, confidence in the method of analysis, difference between test fuel buckling and host lattice buckling, and consistency of results.

The individual results for each test case were then combined using the probable error limits as confidence limits. This allows the results to be weighted by the inverse of the square of the confidence limits. The final result also includes the probable error in the material buckling of the host lattices, taken as $\pm 0.10\ m^{-2}$. These errors were included by statistical addition without weighting. The individual and final results for each test lattice are shown in Table XXIV.

A detailed listing of critical water heights for the PDP buckling measurements is given in Table XXV. The run numbers designate the time sequence. The geometrical configuration of the substituted lattice is that given in Figure 4. The extrapolated water heights, H', are the measured critical water heights plus the extrapolation distances determined by gold pin activation profiles for the reference lattices of Table III. These reference lattices are the one-region lattices of Table XXV. In Table XXV the reference temperature is taken to be 21°C and the reference moderator purity is taken as that of the initial one-region reference lattice for each of the three basic lattices. The temperature corrections are based on HAMMER computations for the reference lattice. Moderator purity corrections are based on plots of measured one-region lattice bucklings as a function of the measured moderator purity. The effect

of slightly different coefficients for the various test lattices is expected to be negligible inasmuch as the statistical weight of the test lattice is small in all cases. Radial dimensions for each of the three basic reactor loads were taken as those for the one-region reference lattice, which was determined for each lattice by gold pin activation profiles. These dimensions are summarized in Table III in terms of radial buckling values.

TABLE XXIV

Summary of PDP Measured Bucklings by Different Methods of Analysis

Coolant	Method of Analysis	Buckling, m^{-2} (a) A	B	C	D	E
		Lattice 1, 19-rod cluster, 9.33-inch pitch				
Air	Two-group	4.50 ±0.40	5.22 ±0.30	7.01 ±0.25	0.15 ±1.00	5.31 ±0.25
	Persson	4.49 ±0.25	5.30 ±0.20	7.25 ±0.20	0.20 ±0.70	5.45 ±0.20
	HERESY	4.65 ±0.25	5.38 ±0.20	7.42 ±0.20	-	5.56 ±0.20
	Result	4.56 ±0.20	5.32 ±0.15	7.26 ±0.15	0.18 ±0.60	5.46 ±0.15
D_2O	Two-group	4.34 ±0.20	5.23 ±0.20	7.09 ±0.20	-0.10 ±1.00	5.28 ±0.20
	Persson	4.35 ±0.20	5.20 ±0.20	7.20 ±0.20	0.26 ±0.50	5.35 ±0.20
	HERESY	4.48 ±0.30	5.30 ±0.20	7.23 ±0.20	0.18 ±0.50	5.38 ±0.20
	Result	4.39 ±0.15	5.24 ±0.15	7.17 ±0.15	0.23 ±0.30	5.34 ±0.15
HB-40	Two-group	-	1.60 ±0.50	-	-1.60 ±0.50	-
	Persson	1.45 ±0.30	1.80 ±0.80	-	-3.25 ±1.00	-
	HERESY	1.60 ±0.40	2.35 ±0.25	-	-1.78 ±1.00	-
	Result	1.50 ±0.25	2.18 ±0.25	-	-2.52 ±0.70	-
		Lattice 2, 31-rods cluster, 12.12-inch pitch				
Air	Two-group	3.86 ±0.40	4.59 ±0.20	6.25 ±0.20	-0.86 ±2.00	4.67 ±0.20
	Persson	3.92 ±0.20	4.62 ±0.20	6.42 ±0.20	0.32 ±0.50	4.70 ±0.20
	HERESY	3.96 ±0.30	4.66 ±0.20	6.41 ±0.30	0.12 ±0.70	4.76 ±0.20
	Result	3.92 ±0.20	4.62 ±0.15	6.35 ±0.15	0.21 ±0.40	4.71 ±0.15
D_2O	Two-group	3.52 ±0.20	4.29 ±0.25	5.98 ±0.20	-0.29 ±1.00	4.40 ±0.20
	Persson	3.52 ±0.60	4.28 ±0.20	6.06 ±0.20	0.20 ±0.35	4.40 ±0.20
	HERESY	3.59 ±0.20	4.30 ±0.20	5.97 ±0.20	1.35 ±0.70	4.42 ±0.20
	Result	3.56 ±0.20	4.29 ±0.20	6.00 ±0.15	0.19 ±0.30	4.41 ±0.15
HB-40	Two-group	0.67 ±0.50	1.03 ±0.20	2.80 ±0.20	-4.40 ±2.00	1.10 ±0.70
	Persson	0.07 ±2.00	1.00 ±0.20	2.70 ±0.20	-3.00 ±1.00	1.00 ±0.50
	HERESY	0.67 ±0.40	1.27 ±0.30	3.00 ±0.30	-2.75 ±1.00	1.35 ±0.70
	Result	0.66 ±0.35	1.06 ±0.15	2.84 ±0.20	-3.04 ±0.70	1.12 ±0.35
		Lattice 3, 31-rods cluster, 9.33-inch pitch				
Air	Two group	3.86 ±0.50	5.25 ±0.50	7.02 ±0.40	-0.81 ±1.00	4.92 ±0.30
	Persson	4.14 ±0.70	4.96 ±0.30	7.19 ±0.35	-0.56 ±0.50	5.02 ±0.20
	HERESY	3.77 ±0.50	5.04 ±0.25	7.32 ±0.25	-0.70 ±0.70	5.05 ±0.20
	Result	3.88 ±0.35	5.03 ±0.20	7.19 ±0.20	-0.64 ±0.40	5.01 ±0.15
D_2O	Two group	3.86 ±0.40	5.06 ±0.20	7.36 ±0.30	-1.27 ±0.70	5.06 ±0.20
	Persson	3.92 ±0.25	4.98 ±0.20	7.25 ±0.20	-1.00 ±0.70	4.99 ±0.20
	HERESY	3.73 ±0.25	4.98 ±0.20	7.23 ±0.20	-1.17 ±0.50	5.00 ±0.20
	Result	3.84 ±0.20	5.01 ±0.15	7.26 ±0.15	-1.15 ±0.35	5.02 ±0.15
HB-40	Two group	1.06 ±1.00	1.42 ±1.00	4.54 ±0.40	-7.52 ±3.00	1.68 ±1.00
	Persson	0.80 ±0.70	2.00 ±0.60	4.55 ±0.30	-5.00 ±1.50	1.50 ±0.70
	HERESY	0.84 ±0.50	2.15 ±0.30	4.62 ±0.30	-4.42 ±1.00	1.91 ±0.40
	Result	0.86 ±0.40	2.07 ±0.30	4.57 ±0.20	-4.75 ±0.80	1.79 ±0.35

(a) For fuel type, see Table I.

TABLE XXV

Critical Water Heights, Temperature, and Moderator Purity Corrections for PDP Substitution Measurements

Lattice 1, 85 19-Rod Clusters at 9.33-inch Pitch

Run	Fuel Type	Coolant	Geom	H', cm	B_z^2, m^{-2}	Temp, °C	Temp Correction, 10^2 m^{-2}	Purity Correction, 10^2 m^{-2}	Purity, mol %	Corrected B_z^2, m^{-2} [a]
2	One-region			227.485	1.90719	21.27	0.14	0	99.565	1.90859
3	B	D_2O	1	228.269	1.89412	21.16	0.08	0.027		1.89519
	B	He	1	227.929	1.89977	21.16	0.08	0.027		1.90084
4	B	D_2O	3A	229.822	1.86861	21.19	0.09	0.054	99.561	1.87005
	B	He	3A	228.850	1.88452	21.19	0.09			1.88596
5	B	D_2O	3S	229.638	1.87161	20.87	-0.06	0.081		1.87182
	B	He	3S	228.738	1.88636	20.87	-0.06			1.88657
6	One-region			227.510	1.90677	20.98	-0.01	0.108		1.90775
7	B	D_2O	7	232.900	1.81953	20.94	-0.03	0.136		1.82059
	B	He	7	230.473	1.85807	20.94	-0.03			1.85913
8 [b]	B	HB-40	3S	247.535	1.61074	20.93	-0.03	0.163		1.61207
9	B	HB-40	3A	248.29	1.60096	20.93	-0.03	0.190		1.60256
10	B	HB-40	7	287.156	1.19692	20.96	-0.02	0.217		1.19889
11 [b]	B	HB-40	3S	247.530	1.61082	20.88	-0.06	0.244		1.61266
12	One-region			227.568	1.90581	20.90	-0.05	0.271	99.560	1.90802
13	A	D_2O	3S	235.137	1.98511	20.92	-0.04	0.298		1.78769
	A	He	3S	234.101	1.80091	20.92	-0.04			1.80349
14	A	D_2O	3A	235.365	1.78164	20.82	-0.09	0.325		1.78399
	A	He	3A	234.224	1.79903	20.82	-0.09			1.80138
15	A	D_2O	1	230.340	1.86022	20.88	-0.06	0.352		1.86314
	A	He	1	229.961	1.86634	20.88	-0.06			1.86926
16	One-region			227.521	1.90658	20.45	-0.27	0.379	99.557	1.90767
17	A	HB-40	3S	253.432	1.53666	20.46	-0.27	0.406		1.53802
18	A	HB-40	3A	254.240	1.52690	20.54	-0.23	0.434		1.52894
19	One-region			227.560	1.90595	20.47	-0.27	0.461		1.90796
20	D	D_2O	1	239.335	1.72302	20.54	-0.23	0.488		1.72560
	D	He	1	239.210	1.72480	20.54	-0.23			1.72738
21	D	D_2O	3A	264.205	1.41391	20.54	-0.23	0.515		1.41676
	D	He	3A	263.431	1.42222	20.54	-0.23			1.42507
22	D	D_2O	3S	264.143	1.41458	20.60	-0.20	0.542		1.41800
	D	He	3S	263.54	1.42105	20.60	-0.20			1.42447
23	One-region			227.670	1.90410	20.60	-0.20	0.569		1.90779
24	D	HB-40	3A	787.532	1.19382	20.64	-0.18	0.596		1.18798
25	D	HB-40	3S	288.575	1.18518	20.70	-0.15	0.623		1.18991
27	One-region			227.750	1.90277	20.41	-0.29	0.678	99.555	1.90665
28	E	D_2O	1	228.365	1.89252	20.41	-0.29	0.705		1.89667
	E	He	1	228.043	1.89786	20.41	-0.29			1.90201
29	C	D_2O	1	224.400	1.96000	20.42	-0.29	0.732		1.96442
	C	He	1	223.982	1.96731	20.42	-0.29			1.97173
30	C	D_2O	3A	218.189	2.07317	20.45	-0.27	0.759		2.07806
	C	He	3A	217.207	2.39123	20.45	-0.27			2.39612
31	C	D_2O	3S	218.714	2.06324	20.30	-0.25	0.786		2.06860
	C	He	3S	217.743	2.08167	20.50	-0.25			2.08703
33	One-region			228.010	1.89842	20.56	-0.22	0.840	99.548	1.90462
34	C	D_2O	7	207.590	2.29028	20.47	-0.27	0.867		2.29635
	C	He	7	205.800	2.33029	20.47	-0.26			2.33636
35	E	D_2O	3A	229.706	1.87049	20.64	-0.18	0.894		1.87763
	E	He	3A	228.820	1.88502	20.64	-0.18			1.89216
36	E	D_2O	3S	229.715	1.86790	20.56	-0.22	0.921		1.87491
	E	He	3S	228.865	1.88428	20.56	-0.22			1.89129
37	E	D_2O	7	231.887	1.83548	20.60	-0.20	0.948		1.84296
	E	He	7	229.647	1.87145	20.60	-0.20			1.88893
38	One-region			228.342	1.89291	20.62	-0.19	0.976	99.543	1.90077
39	B	D_2O	19	241.244	1.69586	20.63	-0.19	1.003		1.70399
	B	He	19	235.540	1.77899	20.63	-0.19			1.78712

(a) The number of figures in these values is not significant. These are only used for difference calculations. See Table XXIV for estimates of buckling error.

(b) Runs 8 and 11 are identical.

TABLE XXV (Continued)

Lattice 2, 85 31-Rod Clusters at 12.12-inch Pitch

Run	Fuel Type	Coolant	Geom	H', cm	B_z^2, m^{-2}	Temp, °C	Temp Correction, 10^2 m^{-2}	Purity Correction, 10^2 m^{-2}	Purity, mol %	Corrected B_z^2, m^{-2}
41	One-region			195.337	2.58662	20.78	0.11	0	99.541	2.58772
42	E	D_2O	1	195.770	2.57519	20.80	0.10	0.066		2.57685
	E	He	1	195.290	2.58785	20.80		0.066		2.58951
43	E	D_2O	3A	196.530	2.55530	20.81	0.09	0.131		2.55751
	E	He	3A	195.245	2.58904	20.81		0.131		2.59125
44	E	D_2O	3S	196.605	2.55335	20.86	0.07	0.197		2.55602
	E	He	3S	195.365	2.58589	20.86		0.197		2.58856
45	E	D_2O	7	198.175	2.51305	20.78	0.11	0.262		2.51677
	E	He	7	195.174	2.59094	20.78		0.262		2.59466
46	One-region			195.491	2.58254	20.83	0.09	0.328	99.540	2.58672
47	C	D_2O	3A	190.513	2.71927	20.86	0.07	0.394		2.72391
	C	He	3A	188.987	2.76341	20.86		0.394		2.76805
48	C	D_2O	3S	199.938	2.70718	20.84	0.08	0.459		2.71257
	C	He	3S	189.506	2.74823	20.84		0.459		2.75362
49	D	D_2O	3S	213.180	2.17173	20.85	0.07	0.525		2.17768
	D	He	3S	212.366	2.18842	20.85		0.525		2.19437
50	D	D_2O	3A	212.762	2.18029	20.88	0.06	0.590		2.18679
	D	He	3A	211.938	2.19727	20.88		0.590		2.20377
51	D	D_2O	1	201.030	2.42768	20.91	0.04	0.656		2.43464
	D	He	1	201.388	2.43351	20.91		0.656		2.44047
52	C	D_2O	1	193.850	2.62644	20.94	0.03	0.722		2.63396
	C	He	1	193.212	2.64384	20.94		0.722		2.65136
53	One-region			195.658	2.57814	20.96	0.02	0.787		2.58621
54	A	D_2O	1	197.205	2.53784	20.96	0.02	0.853		2.54657
	A	He	1	196.720	2.55038	20.96		0.853		2.55911
55	A	D_2O	2A	198.550	2.50358	20.98	0.01	0.918		2.51286
	A	He	2A	197.640	2.52670	20.98		0.918		2.53598
56	A	D_2O	2S	198.400	2.50738	21.00	0	0.984		2.51722
	A	He	2S	197.52	2.52975	21.00		0.984		2.53959
57	B	D_2O	1	196.240	2.56287	21.04	-0.02	1.050		2.57317
	B	He	1	195.771	2.57516	21.04		1.050		2.58546
58	B	D_2O	3A	197.245	2.53682	21.02	-0.01	1.115		2.54787
	B	He	3A	196.000	2.56917	21.02		1.115		2.58022
59	B	D_2O	3S	197.292	2.53561	21.06	-0.03	1.181		2.54712
	B	He	3S	196.030	2.56836	21.06		1.181		2.57987
60	B	D_2O	7	199.542	2.47874	21.10	-0.05	1.246		2.49070
	B	He	7	196.305	2.56118	21.10		1.246		2.57314
61	One-region			195.840	2.57336	21.22	-0.11	1.312	99.540	2.58538
62	E	HB-40	1	200.205	2.46236	20.98	0.01	1.378		2.47624
63	E	HB-40	3S	208.186	2.27720	20.99	0	1.443		2.29163
64	E	HB-40	3A	208.195	2.27699	21.02	-0.01	1.509		2.29198
65	E	HB-40	7	232.618	1.82396	21.08	-0.04	1.574		1.83930
66	One-region			195.915	2.57137	21.14	-0.07	1.640	99.538	2.58707
67	C	HB-40	3S	202.181	2.41448	21.10	-0.05	1.706		2.43104
68	C	HB-40	3A	202.374	2.40985	21.11	-0.05	1.771		2.42706
69	C	HB-40	1	198.260	2.51089	21.11	-0.05	1.837		2.52876
70	A	HB-40	1	201.240	2.43709	21.18	-0.09	1.902		2.45521
71	A	HB-40	2A	206.044	2.32477	21.19	-0.09	1.968		2.24355
72	A	HB-40	2S	205.670	2.33322	21.22	-0.11	2.034		2.35246
73	D	HB-40	1	205.480	2.33756	21.28	-0.14	2.099		2.35715
74	D	HB-40	3A	223.223	1.98072	21.30	-0.15	2.165		2.00087
75	D	HB-40	3S	224.868	1.95180	21.36	-0.18	2.230		1.97230
77	One-region			196.120	2.56602	21.44	-0.22	2.362	99.537	2.58744
78	B	HB-40	1	200.564	2.45356	21.44	-0.22	2.427		2.47563
79	B	HB-40	3S	208.820	2.26337	21.45	-0.22	2.493		2.28610
80	B	HB-40	3A	208.928	2.26105	21.52	-0.26	2.558		2.28403
81	B	HB-40	7	229.096	1.88046	21.58	-0.29	2.624		1.90380
82	B	HB-40	2S	204.533	2.35926	21.58	-0.29	2.690		2.38326
83	B	Air	1	196.375	2.55936	21.59	-0.29	2.755		2.58401
84	One-region			196.286	2.56166	21.62	-0.31	2.821	99.535	2.58677

TABLE XXV (Continued)

Lattice 3, 121 31-Rod Clusters at 9.33-inch Pitch

Run	Fuel Type	Coolant	Geom	H', cm	B_z^2, m^{-2}	Temp, °C	Temp Correction, 10^2 m^{-2}	Purity Correction, 10^2 m^{-2}	Purity, mol %	Corrected B_z^2, m^{-2}
86	One-region			186.027	2.85197	21.48	-0.26	0	99.507	2.84937
87	E	HB-40	1	188.394	2.78076	21.49	-0.26	0.032		2.77848
88	E	HB-40	3S	192.739	2.65680	21.52	-0.24	0.064		2.65504
89	E	HB-40	3A	193.259	2.64254	21.56	-0.22	0.096		2.64130
90	E	HB-40	7	203.207	2.39011	21.58	-0.24	0.128		2.38929
91	B	HB-40	1	188.265	2.78459	21.51	-0.25	0.160		2.78369
92	B	HB-40	3S	192.479	2.66398	21.56	-0.22	0.192		2.66370
93	B	HB-40	3A	192.963	2.65064	21.58	-0.21	0.224		2.65078
94	B	HB-40	7	203.604	2.38082	21.60	-0.20	0.256		2.38138
95	One-region			186.017	2.85228	21.52	-0.24	0.288	99.506	2.85276
96	A	HB-40	1	189.254	2.75557	21.54	-0.23	0.320		2.75647
97	A	HB-40	2A	192.400	2.66617	21.58	-0.21	0.352		2.66759
98	A	HB-40	2S	192.155	2.67296	21.60	-0.20	0.384		2.67480
99	C	HB-40	1	186.546	2.83614	21.61	-0.19	0.416		2.83840
100	C	HB-40	3S	187.275	2.81411	21.20	-0.40	0.448	99.502	2.81459
101	C	HB-40	3A	187.592	2.80459	21.21	-0.39	0.480		2.80549
102	One-region			186.034	2.85178	21.26	-0.37	0.512		2.85320
103	D	HB-40	1	192.761	2.65622	21.19	-0.40	0.540		2.65766
104	D	HB-40	3A	205.675	2.33310	21.20	-0.40	0.576		2.33486
105	D	HB-40	3S	206.049	2.32465	21.22	-0.39	0.608		2.32683
106	B	D_2O	1	186.314	2.84320	21.26	-0.37	0.640		2.84590
	B	He	1	186.297	2.84371	21.26	-0.37	0.640		2.84641
107	B	D_2O	3S	186.790	2.83118	21.30	-0.35	0.672		2.83440
	B	He	3S	186.688	2.83182	21.30	-0.35	0.672		2.83504
108	B	D_2O	3A	186.934	2.82529	21.31	-0.34	0.704		2.82893
	B	He	3A	186.796	2.82855	21.31	-0.34	0.704		2.83219
109	B	D_2O	7	188.004	2.79231	21.37	-0.31	0.736		2.79657
	B	He	7	187.594	2.80452	21.37	-0.31	0.736		2.80878
110	One-region			186.154	2.84810	21.32	-0.34	0.768		2.85238
111	A	D_2O	1	187.376	2.81105	21.33	-0.34	0.800		2.81565
	A	He	1	187.297	2.81344	21.33	-0.34	0.800		2.81804
113	A	D_2O	2A	188.551	2.77616	21.12	-0.44	0.864		2.78040
	A	He	2A	188.390	2.78089	21.12	-0.44			2.78513
114	A	D_2O	2S	188.476	2.77836	21.16	-0.42	0.896		2.78312
	A	He	2S	188.369	2.78149	21.16	-0.42			2.78625
115	One-region			186.197	2.84678	21.18	-0.41	0.928	99.498	2.85196
116	C	D_2O	1	184.612	2.89585	21.24	-0.38	0.960		2.90165
	C	He	1	184.549	2.89786	21.24	-0.38	0.992		2.90398
117	C	D_2O	3A	181.851	2.98446	21.30	-0.35	1.024		2.99120
	C	He	3A	181.747	2.98788	21.30	-0.35	1.024		2.99462
118	C	D_2O	3S	181.904	2.98274	21.32	-0.34	1.056		2.9899
	C	He	3S	181.821	2.98546	21.32	-0.34	1.056		2.99262
119	D	D_2O	3S	199.705	2.47471	21.38	-0.31	1.088		2.48249
	D	He	3S	199.788	2.47263	21.38	-0.31			2.48041
120	D	D_2O	3A	199.714	2.44445	21.52	-0.24	1.120	99.497	2.45225
	D	He	3A	199.709	2.47458	21.52	-0.24	1.120		2.48338
121	D	D_2O	1	199.979	2.70602	21.60	-0.20	1.152		2.71554
	D	He	1	191.004	2.70531		-0.20	1.152		2.71483
122	One-region			186.356	2.84192	21.68	-0.16	1.184		2.85216
123	E	D_2O	1	186.595	2.83464	21.72	-0.14	1.216		2.84540
	E	He	1	186.619	2.83390	21.72	-0.14	1.216		2.84466
124	E	D_2O	3A	187.102	2.81931	21.78	-0.11	1.248		2.82529
	E	He	3A	186.997	2.82247	21.78	-0.11			2.83385
125	E	D_2O	3S	187.020	2.82176	21.86	-0.07	1.280		2.83386
	E	He	3S	186.934	2.82438	21.86	-0.07			2.83648
126	E	D_2O	7	187.973	2.79324	21.89	-0.06	1.312		2.80576
	E	He	7	187.598	2.80442	21.89	-0.06			2.81694
128	One-region			186.451	2.83902	21.86	-0.07	1.376		2.85208

BIBLIOGRAPHY

1. N. P. Baumann. Exponential Measurements on 19-Rod Clusters of UO_2 Rods in D_2O. USAEC Report DP-758, E. I. du Pont de Nemours and Co., Savannah River Laboratory, Aiken, S. C. (1962).

2. A. E. Dunklee. The Heavy Water System of the Process Development Pile. USAEC Report DP-567, E. I. du Pont de Nemours and Co., Savannah River Laboratory, Aiken, S. C. (1961); J. L. Crandall. Status of the United States Effort in D_2O Reactor Physics. DP-787 (1962); J. L. Crandall. Efficacy of Experimental Physics Studies on Heavy Water Lattices. DP-833 (1963).

3. R. C. Axtmann and O. A. Towler, Jr. The Savannah River Exponential Facility. USAEC Report DP-49, E. I. du Pont de Nemours and Co., Savannah River Laboratory, Aiken, S. C. (1954); R. C. Axtmann, et al. Initial Operation of the Standard Pile. USAEC Report DP-32, E. I. du Pont de Nemours and Co., Savannah River Laboratory, Aiken, S. C. (1953) (Declassified 8/29/57).

4. W. E. Graves. Analysis of the Substitution Technique for the Determination of D_2O Lattice Bucklings. USAEC Report DP-832, E. I. du Pont de Nemours and Co., Savannah River Laboratory, Aiken, S. C. (1963).

5. R. Persson. One-Group Perturbation Theory Applied to Substitution Measurements with Void. Report RFX-74, A. B. Atomenergie, Studsvik, Sweden (1961).

6. D. R. Finch. User's Manual for SRL - HERESY I. USAEC Report DP-1027, E. I. du Pont de Nemours and Co., Savannah River Laboratory, Aiken, S. C. (1966).

7. J. E. Suich and H. C. Honeck. The HAMMER System. USAEC Report DP-1064, E. I. du Pont de Nemours and Co., Savannah River Laboratory, Aiken, S. C. (1967).

8. P. Benoist. General Formulation of the Diffusion Coefficient in a Heterogeneous Medium Which May Contain Cavities. Report SPM-522 Commissariat à l'Energie Atomique, Paris, France (1958); P. Benoist. Simple New Expression of the Radial Diffusion Coefficient for Fueled Channels. Report SPM-710 Commissariat à l'Energie Atomique, Paris, France (1962).

9. N. P. Baumann. Process Development Pile Measurements of Lattice Parameters of Natural Uranium in Heavy Water. USAEC Report DP-407, E. I. du Pont de Nemours and Co., Savannah River Laboratory, Aiken, S. C. (1959).

10. D. S. Craig, R. E. Green, and A. Okazaki. "Bucklings from Substitution Experiments by Use of Source-Sink Calculation." Trans. Am. Nucl. Soc. 9, No. 1, 126 (1966).

11. G. F. Kuncir. A Program for the Calculation of Resonance Integrals. USAEC Report GA-2525, General Dynamics Corp., General Atomic Div., San Diego, Calif. (1961).

12. H. P. Flatt. The FOG One-Dimensional Diffusion Equation Codes. USAEC Report NAA-SR-6104, North American Aviation, Inc., Atomics International, Canoga Park, Calif. (1961).

13. H. A. Risti. "Analysis of 7- and 19-Rod UO_2 Cluster Experiments with the HAMMER Code." Trans. Am. Nucl. Soc. 9, No. 1, 517 (1966).

14. E. Hellstrand. "Measurement of Resonance Integrals." Reactor Physics in the Resonance and Thermal Regions, Vol. II p 151-172. MIT Press, Cambridge, Mass. (1966).

15. H. C. Honeck. THERMOS, A Thermalization Transport Theory Code for Reactor Lattice Calculations. USAEC Report BNL-5826, Brookhaven National Lab., Upton, N. Y. (1961).

16. V. Ardente. "Remarks on the Slow Neutron Scattering by Organic Molecules." J. Phys. 641 (1964). See also "Some Theoretical Results Concerning Neutron Thermalization by H Bound in Polyphenyls," by V. Ardente. Paper presented at the Meeting of the Joint Euratom Nuclear Data and Reactor Physics Committee, in Ispra (Feb. 25-26, (1965).

17. N. P. Baumann, P. B. Parks, and D. J. Pellarin. "Spectral Index and Relaxation Length Determinations in Borated D_2O and H_2O", to be published in the Proceedings of the IAEA Symposium on Neutron Thermalization and Reactor Spectra, University of Michigan, Ann Arbor, July 17-21, 1967.

18. P. B. Parks, D. J. Pellarin, N. H. Prochnow, and N. P. Baumann. Thermal Neutron Diffusion in Light and Heavy Water. USAEC Report DP-1090, E. I. du Pont de Nemours and Co., Savannah River Laboratory, Aiken, S. C. (1968).

19. C. H. Westcott. Effective Cross Section Values for Well-Moderated Thermal Reactor Spectra. Chalk River, Ontario, Canada, Reports CRRP-960 (1960); CRRP-662 (1956); CRRP-680 (1957); CRRP-787 (1958), CRRP-862 (1959), and CRRP-960 (1960).

20. L. C. Schmid and W. P. Stinson. "Calibration of Lutetium for Measurements of Effective Neutron Temperatures," Nucl. Sci. Eng. 7, 477-478 (1960). See also HW-70716 p 35 (1961), HW-66319 (1960), and HW-69475 (1961).

21. H. C. Honeck and J. L. Crandall. The Physics of Heavy Water Lattices, USAEC Report BNL-8253, Brookhaven National Laboratory, Upton, N. Y., and E. I. du Pont de Nemours and Co., Savannah River Laboratory, Aiken, S. C. (1964).

22. D. J. Pellarin et al. Zero Power Experiments with ^{235}U-Enriched Thoria and Thorium Metal Lattices for the HWOCR. USAEC Report DP-1125, E. I. du Pont de Nemours and Co., Savannah River Laboratory, Aiken, S. C. (1968).

23. D. A. Brown, Private Communication.